Deep Sea Research Part II: Topical Studies in Oceanography
June 2020, Volume 176, Pages 104806 (18p.)
https://doi.org/10.1016/j.dsr2.2020.104806
https://archimer.ifremer.fr/doc/00631/74286/

Seamount effect on circulation and distribution of ocean taxa in the vicinity of La Pérouse, a shallow seamount in the southwestern Indian Ocean

Marsac Francis [1, 2, *], Annasawmy Pavanee [1, 2], Noyon Margaux [3], Demarcq Herve [1, 2], Soria Marc [1, 2], Rabearisoa Njaratiana [1, 2], Bach Pascal [2, 4], Cherel Yves [6], Grelet Jacques [7], Romanov Evgeny [5]

[1] MARBEC, Univ Montpellier, CNRS, Ifremer, IRD, Sète, France
[2] Institut de Recherche pour le Développement (IRD), Sète, France
[3] UK-SA NRF/DST Bilateral Research Chair: Ocean Sciences & Marine Food Security, Nelson Mandela University, Port Elizabeth, South Africa
[4] MARBEC, Univ Montpellier, CNRS, Ifremer, IRD, Victoria, Seychelles
[5] CAP RUN – CITEB, Le Port, Île de La Réunion, France
[6] Centre D'Etudes Biologiques de Chizé (CEBC), UMR 7372 CNRS-La Rochelle Université, Villiers-en-Bois, France
[7] IMAGO, IRD Bretagne, Technopole de Brest Iroise, Plouzané, France

* Corresponding author : Francis Marsac, email address : francis.marsac@ird.fr

Abstract :

The La Pérouse seamount (60 m depth) has so far been poorly studied despite it being a short distance (160 km) from Réunion Island. As part of the MADRidge project, a multidisciplinary cruise was conducted to evaluate the effect of this shallow seamount on the local hydrology and ecology. Current measurements, temperature and chlorophyll-a profiles, and mesozooplankton and micronekton samples were collected between the summit and 35 km away. Micronekton data were supplemented with stomach content of pelagic top predators as well as fisheries statistics from the domestic longline fleet operating from Réunion. Vertical current profiles revealed distinct patterns between the offshore and seamount-flanked stations, giving evidence of topographical induced flow instabilities, notably on its leeward side (west) relative to the east flank. Distinct patterns in temperature and chlorophyll-a vertical profiles suggest the formation of convergent and divergent circulation cells as a result of the irregular and crescent-like summit topography. Spatial differences in zooplankton abundance were detected with higher biovolumes on the leeward flank. The overall acoustic backscatter for micronekton over the summit was weaker than offshore, but highly concentrated in the upper layer. Albacore tuna and swordfish dominate the longline catch west of Réunion, seemingly in association with a deep (900 m) topographic feature. Yet the largest catch is not directly associated with La Pérouse which would be too shallow for top predators to aggregate around in the long term. Enhanced levels of phytoplankton or zooplankton enrichment at La Pérouse were not demonstrated in this study, nor was there notable diversity of micronekton species. This might explain the relatively limited importance of this seamount to the tuna fisheries in this region.

Keywords : bathymetry, mesoscale eddies, L-ADCP, mesozooplankton, micronekton, stomach contents, pelagic longline fisheries.

1. Introduction

The subsea topography of the South West Indian Ocean (SWIO) is rugged, formed of many banks, ridges (Mascarene Plateau, Mozambique Plateau, Madagascar Ridge, South West Indian Ridge, among others) and isolated seamounts rising from plateaus or from the deep abyssal plains (Tomczak and Godfrey, 1994; Demopoulos et al., 2003; Ingole and Koslow, 2005). The summits of these many seamounts peak at various depths, ranging from >2000 m to just a few metres below the sea surface. Seamounts are known as biodiversity hotspots and are generally rich in demersal and pelagic seamount-associated fish of high commercial value (Fock et al., 2002; Clark et al., 2007). Historically, fish inventories on seamounts worldwide have been developed based on the catches of commercial trawl surveys, such as the Soviet expeditions carried out in the Indian Ocean in the 1970s (Romanov, 2003). Understanding seamount ecosystems was not a priority during this fishing expansion phase. However, following rapid depletion of stocks within a few years of exploitation, in particular stocks of long-lived, slow-maturing species such as the orange roughy (*Hoplostethus atlanticus*) and the alfonsinos (*Beryx* spp.) (Morato and Clark 2007), the need to generate integrated ecosystem

knowledge was recognized in order to develop management and conservation strategies around these seamounts (Rogers et al., 2008; Clark et al, 2012).

The MADRidge project conducted between 2016 and 2017 (see Roberts et al., 2020) was designed to investigate the productivity associated with shallow seamounts, in particular the possible contribution of flow-topographic interactions to enhanced productivity. The project focused on three seamounts located between 19°S and 34°S — (1) La Pérouse (60 m depth), (2) an unnamed pinnacle on the Madagascar Ridge (hereafter named MAD-Ridge, 240 m) and (3) the Walters Shoal (18 m). Multidisciplinary ship surveys were conducted at each seamount. The cruise to La Pérouse was made in September 2016 (DOI: 10.17600/16004500) and aimed to study physical and biological processes that potentially drive important ecological interactions around this seamount, which otherwise is located in an oligotrophic biome — the Indian South Subtropical Gyre (ISSG).

La Pérouse is an extinct volcano rising from the abyssal plain (5000 m depth) up to the surface euphotic layer. Its formation is thought to have occurred 8-10 million years ago, in the same epoch as Réunion (G. Barruol, pers. comm.), as a result of an intraplaque hotspot (Barruol and Sigloch 2013). La Pérouse, as an active volcano, was probably an island in the past. However, due to erosion and seafloor subsidence, it has transitioned to an atoll before becoming a shallow seamount (Deplus et al., 2016). La Pérouse is well-known by recreational fishers who venture to the seamount from Réunion, and by professional fishers operating the Réunion-based longline fleet. Apart from fish resources, significant knowledge gaps exist on the ecosystem and physical environment at and near La Pérouse. The research cruise in 2016 represents the first integrated approach to study the La Pérouse ecosystem.

In this paper, we present and analyse the cruise data that reveal different components of the near and far environment of La Pérouse — including the circulation, hydrology, plankton, micronekton, large pelagic fish and megafauna taxa — to assess whether a “seamount effect” underpins an enhanced ecosystem at this isolated topographic feature on the Mascarene Plain.

2. Material and methods

The R/V *Antea*, owned by the French Institute of Research for Sustainable Development (IRD), was used for the survey. It is a 35-m catamaran equipped for physical and biological investigations in

the coastal and deep ocean. La Pérouse is located 160 km northwest of Réunion, at latitude 19°43'S and longitude 54°10'E (Fig. 1a). The R/V *Antea* left Réunion on 16 September 2016 and took 15 h to reach the study site, which was then investigated for 12 consecutive days. The cruise ended in Réunion on 29 September 2016.

2.1. Bathymetric survey

As several physical and biological measurements were to be done along the slopes of the seamount to study the possible disturbances caused by the topographic rise, it was first necessary to perform a precise bathymetric survey. The GEBCO gridded bathymetric data identifies La Pérouse as an oval-shaped seamount with regular slopes. In 2012/2013, during the RHUM-RUM geophysical cruises on board the R/V *Marion-Dufresne* and R/V *Meteor* (DOI: 10.17600/12200070), the knowledge of seafloor topography in the area was improved by multi-beam surveys along a few transects, showing a more irregular-shaped seamount compared with the GEBCO dataset. However, not all of La Pérouse was surveyed. During our cruise in 2016, a more precise bathymetric survey was conducted using a 12 kHz sounder (SIMRAD EA 500) along latitudinal and longitudinal transects at 1 km intervals over the seamount platform and slopes. This allowed high-resolution mapping of the area with depth data taken every 3 m along the transects. These data were complemented with other depth measurements made with the same echosounder along sampling lines in the survey. In all, 216801 depth measurements were collected over a large area stretching from the summit to 15 km to the north and south, 30 km to the east and 25 km to the west.

This new bathymetric dataset was processed using Golden Software Surfer16® to grid the data across a 20 m mesh to produce a topographic map for the ship survey. The seamount has a crescent-like shape, suggesting that part of the eastern flanks collapsed or that voluminous landslides may have occurred during its formation (Fig. 1b). The existence of a flat top may suggest a drowned reef phase during the seamount's subsidence over time. The platform now lies at 60 m below sea level, and is about 2.5 km wide and reaches 12 km along its largest extension (Fig. 1c).

2.2. Current measurements

Underway current profiles were measured along the Réunion - La Pérouse transit from 16 to 18 September 2016. These data were collected with a 75 kHz RDI Ocean Surveyor II (S-ADCP) using a time average of 2 min. Data were processed using the CASCADE software (Le Bot et al., 2011) which allows flagging and filtering. Measurements were spatially averaged over 5 km intervals for plotting purposes, and restricted to when the ship was moving at constant speed. No tidal correction was applied to these data.

At 11 hydrographic stations (Fig. 1c), profiles of current measurements were collected by two L-ADCPs (RDI 300 kHz) mounted on the CTD frame, one facing up, the other down. This particular configuration maximized the total range of velocity observations, reduced the overall error of the system and provided redundancy of measurements. The raw data from both instruments were combined and then processed using the IFM-GEOMAR/LDEO software version 10.16 (Visbeck, 2001). Data processing corrected the motion and oscillation of the CTD frame, data noise and changes in sound velocity with depth. Ancillary information such as the position (GPS) and the depth (CTD pressure sensor) were imported into the dataset. A tidal correction was first applied to the dataset before aggregating measurements to 8-m depth bins. The zonal and meridian components of the current were transformed to polar coordinates (angle and velocity) and in turn plotted for each station. A vertical direction change index (VDCI) devised by the authors was defined as the cumulative changes in direction of the current between each depth level, in the upper 200 and 400 m respectively:

$$\text{VDCI} = \sum_{i=1}^{n} |(D_{i+1} - D_{i)})|$$

where i is the depth level (8-m intervals) in the 0-200 or 0-400 m layer and D the angle (0-360°) of the current vector. VDCI denotes the degree of disruption in the flow which is directly related to the rotation of the current in the water column. The higher the value, the larger the disruption.

Reprocessed daily L-4 Sea Level anomalies and geostrophic currents were extracted from the CMES (Copernicus Marine Environmental service) database comprising the altimetry data product SEALEVEL_GLO_PHY_L4_REP_OBSERVATIONS_008_047 (http://marine.copernicus.eu) at a spatial resolution of 0.25° of latitude and longitude. These data were used to represent the sea level anomalies and the geostrophic flow during the cruise, and to compute time-series of the daily geostrophic flow at La Pérouse (a square of 3×3 25 km cells) from January 1993 to June 2018.

145

146 2.3. Hydrographic stations

147 Hydrographic surveys were conducted from 21 to 27 September 2016, using a CTD frame
148 equipped with a Sea-Bird 911 Plus CTD and 11 Ocean-Test bottles (8 L Niskin type). In all, 11 CTD
149 casts were done from the surface to a maximum depth of 1500 m (or as close to the bottom as
150 possible) (Fig. 1c). The CTD measured depth, temperature, conductivity, dissolved oxygen and
151 fluorescence. Water samples were collected at three depths at all stations for the analytical
152 determination of salinity and dissolved oxygen. Nutrient samples were collected at six depths, or
153 more, and pasteurized on board for later analysis using an AXFLOW AA3 continuous flow analyser in
154 the laboratory (IRD, Brest, France). Four litres of seawater were filtered to collect pigments (filters
155 preserved at -80°C) at four or five different depths, namely: surface, mixed layer, depth of maximum
156 fluorescence (given by the CTD Fluorometer (Wetlabs® ECO-FLNTU) and below the thermocline, so
157 as to cover a wide range of values.

158 Chlorophyll-*a* (Chl *a*), the only pigment used in this study, was later measured in the laboratory
159 using High Performance Liquid Chromatography (HPLC). The analytical determination of salinity,
160 dissolved oxygen and Chl-*a* was used to calibrate the CTD measurements. Several proxies were
161 computed from the calibrated CTD profiles. We *inter alia* used the depth of 'Temperature at 5 m
162 minus 1°C' as a criterion to define the mixed layer depth (MLD) (Sprintall and Cronin, 2009). The
163 depth at which the sum of nitrate and nitrite concentrations reached 1 μmol kg^{-1} was used to determine
164 the depth of the nutricline using a linear interpolation between consecutive sampling depths (Dufois et
165 al. (2014). The deep chlorophyll maximum (DCM) is defined as the depth where the peak chlorophyll
166 value is found. Finally, the integrated Chl-*a* is the sum of the chlorophyll concentrations of the upper
167 200 m of the water column.

168 Four stations located away from the seamount were aligned with the cardinal directions — North,
169 South, West and East (i.e. 1, 2, 8, 10 respectively), and ranged between 10 and 21 km from the
170 seamount platform (70 m isobaths). These served as control stations and hereafter are referred to as
171 'Offshore' stations. By contrast, seven stations (hereafter 'Flank' stations) were distributed from 1.1 to
172 3.2 km around the seamount platform (ranging in depth from 800 to 1200 m, except for station 5 at

300 m) which enabled investigation into the possible influence of the seamount on the hydrology of the water column. All stations were then classified accordingly as 'Offshore' or 'Flank' (see Table 1).

2.4. Zooplankton sampling

Mesozooplankton samples were collected at each hydrological station in the upper 200 m using a 200-µm-mesh Bongo net (0.25 m² mouth area), equipped with a flowmeter and connected to an underwater recording unit (attached to the frame). A V-fin depressor hanging below the Bongo frame allowed the nets to remain correctly orientated during the oblique tows at a vessel speed of 1.5-2 knots. The samples were preserved in buffered formaldehyde (4% final concentration). In the laboratory, each sample was split until the subsample contained approximately 1000-2000 particles. This subsample was then scanned using a ZooScan (Hydroptics) following the procedure described in Gorsky et al. (2010) and Vandromme et al. (2012). An ellipsoid estimated the biovolume of each organism with a pre-existing training set and the random forest algorithm was used for pre-sorting of the particles with the online platform Ecotaxa (Picheral et al., 2017). The classification of each organism was verified manually. Only the biovolume of organisms (in mm^3 m^{-3}) is analysed in this study. Zooplankton were not sampled at station 5 because of its shallowness. All Bongo samples were collected in daylight.

2.5. Acoustic survey

Acoustic data were collected by both day and night along transects using a 4-frequency Simrad EK60 echosounder (38, 70, 120 and 200 kHz) at a vessel speed of 8-9 knots. The pulse duration was set to 0.512 ms. The water column was sampled to a depth of 740 m during data acquisition using the 38 kHz frequency (transmitted power of 1000 W), which is the only frequency used in this paper because of the larger vertical range relative to the other frequencies. These acoustic data were processed with the Matecho software (Release 2010b), which is based on IFREMER's Movies3D software (Trenkel et al., 2009, Perrot et al., 2018), and considered an open source IRD tool (computed with MATLAB 7.11.0.184). Background noise, bottom echoes and attenuated signals were removed using algorithms designed by De Robertis and Higginbottom (2007) and Ryan et al. (2015). The first

10 m below the sea surface was removed due to over-amplification of the acoustic signal by surface bubbles. The along-track sampling unit was 0.1 nautical mile (1 nmi = 1852 m). Echo-integration was performed at a Sv threshold of −80 dB with 1 m layers intervals. The micronekton acoustic density was determined by the nautical area scattering coefficient (NASC, or Sa, m^2 nmi^{-2}, related to the backscattered energy), which defines a proxy of the relative biomass of micronekton, provided certain assumptions are met (Béhagle et al., 2014). The water column was split into three depth categories: 10–200 m (surface layer), 200–400 m (intermediate layer) and 400–740 m (deep layer), following an initial analysis of the echograms, which indicated that organisms were organized vertically into these three main strata. Transects were grouped in distinct spatial domains from the seamount in order to compare the acoustic densities between domains. Daylight transects were distributed in two domains: 'Vicinity' (3-10 km off the seamount platform) and 'Summit and flank' (<3 km), while two night transects located at 23 and 35 km east and west of the summit, respectively, defined a third domain named 'Offshore' (Fig. 8a later). Here, the 'Summit and flank' category, which extends down to 1000 m along the flanks, overlays the 'Flank' category used for hydrological stations and Bongo nets, and the summit platform of La Pérouse.

2.6. Micronekton sampling

The first set of micronekton samples was collected during the La Pérouse cruise using a 40 m-long International Young Gadoid Pelagic Trawl (IYGPT) net, constructed of 8 cm knotless nylon delta mesh netting at the front tapering to 0.5 cm at the codend (theoretical maximal mouth opening of ~96 m^2). The trawl was towed at a speed of 3-4 knots for 1 h. Trawl depth was monitored using a Scanmar depth sensor. Trawl 5 located over the summit was the only one conducted during daylight. The other nine trawls were performed during night-time at various depths, with maximum depths ranging from 60 to 590 m (Fig. 1c and Table 2). Night trawls were operated mostly after 18:00 local time (twilight). Midwater trawls were performed to sample the diversity of micronekton organisms and establish links with the acoustic densities at the different layers. With seven trawls in the 'Vicinity' area and one in each of the 'Summit', 'Flank' and 'Offshore' areas — trawl data were not used to compare areas.

To place the trawl composition of micronekton at La Pérouse in a broader context, we used unpublished information on fauna identified in the stomach contents of top predators, caught by the commercial longline fleet based in Réunion. This complementary, historical dataset was collected by several projects over the past 10 years: IOSSS (Ifremer) in 2009, PROSPER (CAP RUN, IRD) in 2010-2011, DCF-DCMAP (IRD, CAP RUN) in 2012, RAF (CAP RUN, IRD) in 2012-2013, GERMON (Ifremer, IRD, CAP RUN) in 2014. To add to this, stomach contents of three predators were also sampled around La Pérouse during the 2016 cruise. This entailed a final dataset consisting of 93 non-empty stomachs belonging to six top predator species: three tuna species (albacore *Thunnus alalunga*; yellowfin *T. albacares* and bigeye *T. obesus*), swordfish (*Xiphias gladius*), dolphinfish (*Coryphaena hippurus*) and longnose lancetfish (*Alepisaurus ferox*) (Table 3).

The spatial distribution of the longline sets allowed us to discriminate two regions based on the distance from the seamount. A distance of 20-40 km was considered the radius of influence of La Pérouse on the large pelagic fisheries (Morato et al, 2008, 2010). The stomachs collected within 10 km of La Pérouse were in the 'Vicinity' area, and those collected from 75 to 280 km were assigned to the "Open-ocean area" (Fig. 1a). However, all sets located within a radius of 90 km from Réunion were excluded to minimize any island effect in the micronekton composition. There were 12 stomachs in the 'Vicinity' area, and 81 in the 'Open-ocean' area (Table 3). The spatial stratification across the different data components of this study is summarized in Table 4.

Prey items were identified to the lowest possible taxon using the most recent guides for each group. Identification of highly digested prey remains was based on the diagnostic hard parts (e.g. otoliths for fish, beaks for cephalopods). For each stomach, the number (N) and occurrence (O) of each species were recorded. The reconstituted weight (RW), using only fresh remains, was estimated from allometric equations relating dimensions of identifiable hard parts to the weight of the species using our own relationships or presented in the literature (Clarke, 1986; Smale et al., 1995; Lu and Ickeringill, 2002; Potier et al., 2011; E.V. Romanov unpublished). For each identified prey item, the mean proportion (%) for both number (MN) and reconstituted weight (MRW) were calculated by considering the proportion of each prey species (or taxa/category) found in the individual stomachs. Finally, the average species contributions to prey composition across all stomachs were calculated by

area, as previously defined. We therefore treated individual stomachs as the sampling unit, allowing us to compute standard deviation for species relative to the stomachs' statistical population (Chipps and Garvey, 2007). An index of relative importance (IRI; Pinkas et al., 1971) was calculated to combine all three measures into a single estimate of the relative importance of food types:

IRI = %O x (%MN+%MRW)

from which percentage values were used for comparison:

$$\%IRI = 100 \sum_{i=1}^{n} IRI_i$$

2.7. Large pelagic fish indicators

No fishing operations targeting top predators were carried out during the cruise. Rather, catch and effort (C/E) fisheries statistics available in the international database of the Indian Ocean Tuna Commission (IOTC) (www.iotc.org/data-and-statistics) were used to investigate fisheries production in the proximity of La Pérouse. The approach compared catch distribution throughout the entire South West Indian Ocean. Only statistics from the Réunion domestic longline fleet were selected because it is the only longline fleet reporting catch and effort on a 1° grid. Asian longline fleets in the area report on a 5° grid resolution, which is too coarse to investigate seamount effects on the catch. First the nominal catches were compared with the C/E statistics to verify the amount of spatial reporting. It was found that 100% of the fished squares are indeed reported in the database. Four species accounting for 94% of the total catch were examined: three tuna species (yellowfin, bigeye and albacore) and swordfish. Catch by species (metric tons) and effort (number of hooks deployed) were summed per 1° grid cell over the period 2009-2017 to produce average maps.

2.8. Marine mammals and seabird observations

Visual census of marine mammals at the sea surface was conducted from the top deck of the research vessel. Species identification, group size estimate, time and position were recorded. Sighting positions were obtained from a global position system (GPS). The visual effort (duration) was also recorded. During the 14-day cruise, only 46 h of observations during just five days were undertaken due to rough sea conditions.

3. Results

3.1. Altimetry and regional circulation

The altimetry field covering the region between Réunion and La Pérouse, for the duration of the cruise, was characterized by moderate geostrophic gradients not exceeding 0.36 m (Fig. 2; sea level anomalies ranged from -0.26 m to +0.10 m). During the first part of the cruise (16-25 September), La Pérouse was located on the edge of a cyclonic eddy which moved towards the northwest at an average speed of 12 km d^{-1} (Fig. 2a). From 16 to 18 September 2016, the S-ADCP measurements between Réunion and La Pérouse indicated high current velocities (50-90 cm s^{-1}) over a distance of some 55 km (20.5°S to 20°S) in the upper 180 m (Fig. 3a), in a northwesterly direction along the sea level gradient seen at the edge of the cyclonic eddy. During the last few days of the cruise (26-29 September), the eddy field had changed with a southerly, lower velocity, geostrophic flow moving over La Pérouse (Fig. 2b). This was confirmed by the S-ADCP measurements between 28 and 29 September 2016 (i.e. 30-50 cm s^{-1}) (Fig. 3b). Statistics, calculated from the daily CMEMS altimetry data product from January 1993 to June 2018, show the geostrophic flow at La Pérouse to exhibit daily variations ranging from 2 to 55 cm s^{-1} with a median of 16 cm s^{-1}.

3.2. Current measurements

3.2.1 L-ADCP profiles at offshore stations

The four 'Offshore' stations were located on the North (1), South (2), East (8) and West (10) of the seamount. Current velocities in the layer 0-1000 m are displayed in Fig. S1 (Supplementary information). It is seen that stations 1 and 2 exhibited a similar vertical structure in the upper 350 m. Flow was in a northwesterly direction in the upper 150-200 m (30-54 cm s^{-1}) and gradually rotated to the west, reaching a depth of 300 m. Below 400 m, the current was eastwards at station 1 (9-20 cm s^{-1}), but in comparison, southwards then eastwards for the same depth range at station 2 (5-11 cm s^{-1}). At station 8, the vertical current structure was northwesterly in the upper 200 m, similar to station 1 with lower velocities (20-26 cm s^{-1}). From 300 to 700 m, the flow was eastwards, i.e. in an opposite

direction to that in the upper layer (8-22 cm s^{-1}). Station 10 was very different from the other three 'Offshore' stations. This was undertaken during the last part of the cruise, and showed an easterly current in the upper 150 m with the weakest velocities of all 'Offshore' stations (8-16 cm s^{-1}). The sudden rotation of the current at station 10 coincided with a sharp pycnocline at 150 m (Fig. S1).

3.2.2 L-ADCP profiles at flank stations

None of the seven profiles conducted on the slopes of the seamount showed the same vertical pattern (Fig. S2). Two groups are considered here, namely stations 3, 4, 5, 6 and 7, that were sampled on 23 September, and stations 23 and 24 sampled on 27 September, which coincide with the change in the main surface flow in Fig. 2. Currents appear to be layered in the vertical axis. Average velocities are hereafter reported with 1 standard deviation.

At station 3, the current was highly unsteady in the upper 200 m. The flow was northwards above 100 m (average 23.6 ± 5.9 cm s^{-1}) and rotated clockwise (cyclonic) from northeast to southwest in the layer 100-200 m (average 6.2 cm s^{-1}). From 200 to 260 m, the flow was northeastwards with a sharp reversal to the west until 400 m. At station 6, the current was strong and steady to the west to a depth of 150 m (average 24.5 ± 5.5 cm s^{-1}), where a sharp pycnocline (24.4-25) was observed. Below the pycnocline, in a layer of about 100 m, the current rotated anti-clockwise (anticylonic). The current turned gradually from eastwards to southwards in the layer 250-575 m. At station 7, the flow was northwestwards in the upper 60 m (average 17 ± 2.7 cm s^{-1}), then rotated clockwise (cyclonic) to the east from 100 to 175 m. Below 200 m, the current remained more or less in the same direction (northwest). Station 5 on the upper slope of the seamount (200 m bottom depth), was characterized by a high velocity (up to 52 cm s^{-1}) westward flow in the upper 50 m. This then rotated and sharply decreased in velocity near the bottom. Station 4 showed a high velocity (average 37.1 ± 9.3 cm s^{-1}) towards the northwest in the upper 70 m, then rotated slightly to the northeast down to 110 m. A sudden directional change (to the west) was observed at 130 m, the same depth at which a strong density gradient was observed (24.6-25.0). Deeper, the current was steady in direction, keeping a dominant northward component.

The flow in the upper 100 m at both stations 23 and 24 was well established towards the south (average of 25.1 ± 3.7 and 24.2 ± 9.2 cm s^{-1}, respectively). Southward flow was observed down to 200 m at station 23, while a westward flow developed within a thin layer (128-144 m) in association with a rapid isopycnal change (24.2-25.0) at station 24. At station 23, the flow was unstable in direction from 300 to 400 m with a dominant northward component in the deeper layers. Flow at station 24 was predominantly eastwards from 160 to 250 m, followed by westwards to 500 m.

3.2.3 Statistical comparison between offshore and flank stations

'Offshore' and 'Flank' stations were compared in terms of velocity and directional changes, in both the 0-200 m and 0-400 m layers. The full paired Wilcoxon test results for these comparisons are provided in Tables S1 and S2 (Supplementary information). Velocities are examined first. Within the 'Offshore' stations in the upper 200 m, only stations 1 and 2 were statistically similar ($p > 0.05$) with higher velocities (median of 35.7 and 40.4 cm s^{-1}, respectively) than at the other two 'Offshore' stations (25.2 and 14 cm s^{-1} for stations 8 and 10, respectively) (Fig. 4a). In the upper 400 m, stations 1 and 2 were also statistically different from stations 8 and 10 ($p > 0.05$) with a generally lower current velocity along the flanks of the seamount (Fig. 4b). In both layers, the 'Offshore' stations had a significantly different vertical velocity pattern from the 'Flank' stations. Statistical different patterns were observed in 75% of the paired tests in the upper 200 m and 83% in the upper 400 m (Table S1).

Variability in the flow direction throughout the water column was similar at 'Offshore' stations 1, 2 and 8 in both depth ranges ($p > 0.05$), with few directional changes (Table S2). Station 10 (which was affected by the westward eddy displacement) exhibited more changes in direction relative to the other 'Offshore' stations (except some similarity with station 1 in the 0-400 m layer; $p > 0.05$). The directional change also differed between 'Offshore' and 'Flank' stations, as observed in 78% and 63% of the cases for the layers 0-200 m and 0-400 m, respectively (Table S2).

A vertical directional change index (VDCI) was computed to assess the extent of current rotation with depth (Table 5). For three of the 'Offshore' stations (1, 2 and 8) the VDCI exhibited the lowest values among all stations. Seamount stations had higher VDCIs than 'Offshore' stations. In the upper 400 m, stations 3 and 23, both located on the western flank, had the highest VDCI with station 3 being

ranked first. In the range 0-200 m, station 3 had the second highest VDCI after station 5 (eastern flank at a shallow depth, 200 m, along the slope). Stations 7 and 24, located in the southwest corner of La Pérouse, showed intermediate VDCI values in both depth ranges. Station 23, located on the western flank, had the lowest VDCI in the 0-200 m depth range and, by contrast, was the second highest in the 0-400 m depth range, denoting a rather stable direction of the flow in the upper 200 m and a highly disrupted flow beneath, as shown in Figure S2. Stations 6 (southwest flank) and 4 (eastern flank) exhibited weak VDCI across both depth ranges.

3.3. Hydrology and chlorophyll concentration

The 11 hydrological stations (Fig. S3) were pooled into three groups by visual examination of the temperature profile shape and depth of the mixed layer (Fig. 5a-c). Group 1 comprised 'Offshore' stations, where the MLD is found between 100 and 130 m and the thermocline less pronounced than in group 2 (Fig. 5a). Groups 2 and 3 are for the 'Flank' stations. Group 2, consisting of stations 3, 23 and 7, showed a MLD between 80 and 89 m (Fig. 5b). The temperature gradient at the bottom of the MLD was weak, as temperature decreased in a quasi-continuous linear trend below 50 m. By contrast, Group 3 comprising stations 4, 24 and 6, had a well-defined and deep thermocline at 150 m (MLD ranges between 91 and 136 m, Fig. 5c). The surface warming seen at stations 23 and 24 was due to calm weather conditions on 26 and 27 September, not experienced at any other time during the cruise.

Relative to temperature, the fluorescence profiles showed a greater within-group heterogeneity (Fig. 5d-f). In Group 1, the maximum chlorophyll concentration (Fmax) ranged widely between 0.19 and 0.4 mg m^3 with a DCM fluctuating between 115 and 141 m (Fig. 5d). In Group 2, the Fmax was twice as high at stations 23 and 7 (0.4 mg m^3 and above) than at station 3 (0.19 mg m^3) and the DCM fluctuated between 65 and 86 m (Fig. 5e). In Group 3, the Fmax was relatively low (0.25-0.32 mg m^{-3}) and the DCM was deeper than in Group 2 stations, between 65 and 108 m (Fig. 5f). The position of the DCM was closely associated with the nutricline for 'Offshore' and 'Flank' stations ($r_{sp} = 0.92$; $p < 0.05$) with Fmax located a few metres above the nutricline.

MODIS surface Chl-*a* concentration, averaged between 23 and 27 September, was observed to be slightly higher in the proximity of the seamount than in the surrounding waters (Fig. S4). The

distribution was patchy around the seamount, with higher concentrations over the northern platform and slopes than on the southern part. Nonetheless, the range of Chl-*a* concentration (0.02--0.08 mg m^{-3}) was relatively low and characteristic of an oligotrophic environment. A detailed comparison with other seamounts in the SWIO is given by Demarcq et al. (2020).

3.4. Zooplankton

The 10 net tows were classified into three groups according to total biovolume, namely Offshore (4 tows), Western flank (4 tows) and Eastern flank (2 tows) (see Fig. 6). A Kruskal-Wallis ANOVA test (KW) indicated that all three groups were significantly different ($H = 7.85$, $p < 0.05$), with the highest biovolume recorded along the western flank (median = 59 mm^3 m^{-3}), the smallest along the eastern flank (23.4 mm^3 m^{-3}) and intermediate values at the offshore tows (38.9 mm^3 m^{-3}). The relatively high biovolume measured at station 7 should be regarded with caution as it was the only tow with organisms >4 mm. These comprised large Trachymedusa (Noyon et al., 2020). Overall, the zooplankton biovolume was inversely related to the integrated Chl-*a* concentrations in the upper 200 m (Fig. 7). The range of zooplankton biovolume and integrated Chl-*a* on the flank tows were distributed over a wide range of values relative to those for the offshore tows (1, 2, 8, 10). The correlation between the biovolume and the integrated Chl *a* was highly significant for the flank tows ($r_{sp} = -0.94$, $p < 0.05$).

3.5. Micronekton acoustic densities along transects

The night-time acoustic density for the entire water column was significantly greater than in daylight for all transects (1025 and 499 m^2 nmi^{-2}, respectively, Wilcoxon rank sum test, $W = 1311$, $p < 0.05$). However, the daylight acoustic density, similarly for the entire water column, was significantly different across all transects (Fig. 8b) (KW, $H=185.49$, $df=12$, $p < 0.05$). Transects carried out to the east (East 2 and 3), northeast and in the western extremity (West 3) of the seamount showed higher daylight acoustic densities (589-635 m^2 nmi^{-2}) than all the other transects (336-499 m^2 nmi^{-2}) (Fig. 8b). For almost all transects, the deep scattering layer was denser than the surface (52.3% vs 41.8% on average). The 'Summit and flank' area exhibited the lowest overall acoustic densities, although the

proportion in the surface layer was the highest by day (59%, similar to the southwest transect which was located close to the slope).

In a similar way to daylight, the night-time acoustic responses of the whole water column also differed significantly across all transects (Fig. 8c) (KW, $H = 182.18$, $df = 11$, $p < 0.05$). The transects in the vicinity of the seamount exhibited the highest acoustic densities, whereas the lowest values were found on the 'Summit and flank' area of the seamount. Most of the night-time acoustic signal was located in the surface layer, which represented 87% of the total acoustic density on average. The highest proportion (98%) of surface layer relative to the total acoustic response at night was again recorded at the 'Summit and flank' transects.

Over the 'Summit and flank', the distribution of the daylight and night-time acoustic responses of the total water column was asymmetrical with a strong positive skewness (Fig. 9). Such a distribution was significantly different (with a lower median) from that of the 'Vicinity' area (KW, $H = 66.3$, $df = 1$, $p < 0.05$). At night, significant differences were also found between the 'Summit and flank' and the 'Vicinity' and 'Offshore' areas (KW, $H = 98.44$, $df = 2$, $p < 0.05$), which were also significantly different ($p < 0.05$) (Fig. 9).

Echograms of the 38 kHz frequency showed aggregations of organisms closely associated with La Pérouse's summit in the top 100 m by day (Fig. 10a). A secondary scattering layer was located below 400 m during the day, whereas at night, the surface scattering layer was intensified in the upper layer of the water column and therefore over La Pérouse summit (Fig. 10b).

3.6. Composition of micronekton around La Pérouse

3.6.1 Trawl sampling

The best represented group in trawl landings, both in number (36%) and mass (54%), were fish. Overall, 77 taxa were caught (2272 fish) belonging to 19 families (Cherel at al., 2020). The gelatinous micronekton was the second most abundant group (33% in number and 24% in mass) at La Pérouse followed by crustaceans (24% in number and 10% in mass) and cephalopods (7% in number and 12% in mass). Fish were dominated by myctophids (49%), the most diverse family with 28 species. The second most represented family was the gonostomatids (21%), with three species (see Cherel et al.,

2020, for more detail on the taxonomic composition of the trawls). Cephalopods and crustaceans delivered 10 and 12 species, respectively.

2.6.2 Stomach content analyses

Fish was the principal prey item in the stomach contents of pelagic top predators in both the 'Vicinity' and 'Open-ocean' areas: 53.7% and 44.6% of IRI respectively (Table 6). Fish prey were dominated by myctophids in both areas. Unidentified fish (apparently poorly identified groups of demersal species) were largely represented in stomach contents at La Pérouse vicinity (29.8% of IRI, 16.0 ± 31.2% of MRW).

Crustaceans were the second most important prey group in the vicinity of La Pérouse and found in lesser abundance in stomachs in the 'Open-ocean'. Cephalopods showed an opposite pattern, with high importance in the 'Open-ocean' area both in terms of IRI (40.3%) and MRW (41.5%), and low importance at in the vicinity of La Pérouse (15.8% of IRI but 41.8% of MRW owing to the occurrence of few large squid) (Table 6). Among the 'Open-ocean' squid, the onychoteuthid whale squid *Walvisteuthis rancureli* was the second most important prey item (18.8% of IRI, 6.6 ± 29.2% of MRW) followed by purpleback flying squid *Sthenoteuthis oualaniensis* (Ommastrephidae) (9.8% of IRI and 4.3 ± 14.2% of MRW).

In the 'Vicinity' area, besides the identified fish taxa, prey species comprised of post-larvae reef lobster *Enoplometopus* spp. (14.6% of IRI, 15.3 ± 31.8% of MRW), non-identified fish and fish larvae (9.3% of IRI, 4.5 ± 10.5% of MRW), post-larvae of the stomatopod *Odontodactylus scyllarus* (6.9% of IRI, 4.2 ± 12.3% of MRW), adult hyperiid amphipods (*Platyscelus ovoides*, 5.6% of IRI and 2.7 ± 6.8% of MRW) followed by whale squid (5.3% of IRI, 11.0 ± 26.3% of MRW) and argonauts (*Argonauta argo)* (4.9% of IRI, 7.9 ± 18.6% of MRW). Contrasts between high IRI and low MRW values (e.g. crustaceans and juvenile fish) are related to high numerical abundance and common occurrence of prey with low individual weight.

3.7. Distribution of large pelagic catches

The Réunion domestic longline fleet mostly operate in the Mascarene basin in the ISSG province, between Réunion and Madagascar (latitudes 16-27°S). Maps of catch by species and fishing effort

(number of hooks) are shown in Fig. S5. The fishery is characterized by two core zones: (1) the east coast of Madagascar (19-23°S) and (2) an area west of Réunion and south of La Pérouse (19-22°S, 54-55°E). Some species-specific patterns stand out. Yellowfin tuna catches are of the same magnitude in both areas. Bigeye tuna are essentially caught east of Madagascar whereas albacore and swordfish are mostly exploited west of Réunion. To quantify the relative importance of large pelagic catches in the area close to La Pérouse, we calculated the proportion of catch taken by month in the two 1° squares adjacent to La Pérouse (19-21°S, 54-55°E) (Fig. S6). On average, the proportion ranged between 10 and 15% during the summer peak fishing season (November-February). The catch pattern follows that of fishing effort. Among these species, albacore yielded the highest catch in the proximity of La Pérouse mostly all year round, with exceptions in November and December when it is surpassed by yellowfin and bigeye tuna. However, the fishing maps in Figure S5 also show the largest catches for albacore and swordfish from square 21-22°S, 54-55°E located some 100-150 km south of La Pérouse. Interestingly, another deeper topographic rise, known as 'Clé à molette' by the fishers, is found there. This has a summit around 900 m deep and contributes 15% of the Réunion fleet catch between November and January.

3.8. Observations of megafauna

During the entire cruise, the only marine mammal sighting was a group of two baleen whales. The sighting was too distant to allow accurate species identification. For seabirds, a total of 40 sightings was recorded. The most frequently encountered seabirds were Barau's petrels (*Pterodroma baraui*) with 10 sightings (12 individuals), and sooty terns (*Onychoprion fuscatus*) with 8 sightings (29 individuals). Roseate terns (*Sterna dougallii*) and brown noddies (*Anous stolidus*) were the least commonly sighted — 2 sightings (13 individuals) and 2 sightings (62 individuals), respectively. Other observations of seabird species included wedge-tailed shearwater (*Puffinus pacificus*), white tailed tropicbird (*Phaeton lepturus*) and Audubon shearwater (*Puffinus lherminieri*).

4. Discussion

The research cruise carried out in September 2016 around La Pérouse covered many aspects of the seamount ecosystem (topography, hydrology, plankton and micronekton distribution) and generated new datasets on a poorly known topographic rise, only discovered in 1962. The high-resolution map of La Pérouse produced during this cruise gave evidence of a crescent-shaped summit, possibly as a result of a huge landslide that occurred on its eastern flank in the distant past. The newly acquired knowledge of the irregular shape of the summit is potentially key to understanding the circulation pattern around the seamount.

4.1. Seamount influence on local circulation

The current profiles revealed very different patterns between the 'Offshore' (control) and 'Flank' stations. 'Offshore' stations 1 and 2 (north and south of the study area) were statistically similar with a current flowing to the west-northwest in the upper 250 m at a speed of about 36.3 cm s^{-1}. These measurements reproduced the regional current pattern depicted by the S-ADCP during the transit from Réunion to La Pérouse, between 16 and 18 September (Fig. 3a). This was also in agreement with the altimetry field (Fig. 2a) indicating a sustained westward geostrophic current along a sea level gradient between a cyclone and an anticyclone located northeast and southwest of La Pérouse, respectively. At station 8 (western station, sampled on 25 September) the flow velocity was lower than at stations 1 and 2, with an average of 24.9 cm s^{-1}. Station 10 (eastern station sampled on 26 September) was distinct from the other three 'Offshore' stations with a low speed and eastward flow (average of 13.8 cm s^{-1}). This change in current pattern is caused by the evolving altimetry field (Fig. 2b), as confirmed by S-ADCP measurements on the return transit from La Pérouse to Réunion, on 28 and 29 September (Fig. 3b). Stations 8 and 10 reflect this displacement of the eddy field. Then, during the last days of the cruise, two key observations were made, viz.: (i) the altimetry gradient was reduced, resulting in weaker currents; and (ii) station 10 being in the easternmost position was more influenced by the ongoing changes than station 8 in the westernmost position. The effect of the changing eddy field also affected the 'Flank' stations. At stations 3-7 (23 September), the flow was mostly northwesterly, but southerly at stations 23 and 24 (27 September), when the eastern limb of the cyclone was reaching La Pérouse.

The 'Flank' stations showed a larger range of current velocities and directions than the control stations, giving evidence of flow instabilities caused by the seamount slopes within a distance of some 3 km from the summit platform. Current rotation through the water column was the most obvious flow disturbance, at times associated with the pycnocline. In general the VDCI was higher at the 'Flank' stations than at 'Offshore' stations. In the upper 400 m, the highest value was found at stations 3 and 23, both located on the western slopes (leeward side of the summit). In contrast, station 6 had the least turbulent flow, likely owing to it being the farthest 'Flank' station. These findings clearly indicate that topographic-induced turbulence in the water column is higher on the leeward side of the seamount, and diminishes with distance from the summit. Furthermore, changes in the direction of flow below the seamount summit, i.e. between 100 and 120 m on the eastern flank (stations 4 and 24), show currents to follow the seamount shape.

Deflections of the impinging flow caused by a seamount is a common phenomenon, well-described by observations and models (Mohn et al., 2009, Lavelle et al., 2010). Taylor columns, trapped and closed circulations around an obstacle (Taylor, 1923; Hogg, 1973; Huppert, 1975, Huppert and Bryan, 1976), can only be generated under specific conditions of current speed, water column stratification and topography. The resulting circulation is anticyclonic which causes trapping of upwelled water in the water column above the summit, with implications for the local biology (Genin and Boehlert, 1985; Pitcher and Bulman, 2007). In this regard, vertical flow components observed around La Pérouse do not show any pattern suggesting the existence of a Taylor column there, certainly at the time of the cruise. This is not surprising. We recall that the theoretical calculation to determine whether or not a Taylor column can form at a seamount depends on two metrics, the Rossby number (Ro) and the relative height of the seamount relative to the ocean depth (α) (Chapman and Haidvogel, 1992, White et al., 2007). Both metrics are used to calculate a blocking parameter (Bl) which determines the potential for the generation of a Taylor column over tall seamounts (when $\alpha > 0.4$, $Ro < 0.15$ and $Bl > 2$, see Chapman and Haidvogel, 1992). In the case of La Pérouse, the calculation does not support the formation of a Taylor circulation around its summit (Annasawmy et al., 2020c). Moreover, in reality, the complex crescent-shaped seamount summit,

562 combined with bathymetric protrusions on its flanks, prevent water circulating around the summit with
563 steady anticyclonic motion, i.e. formation of a Taylor column.

564 It is interesting, that a weak Taylor column was evidenced by direct current measurements at the
565 shallow Cobb seamount (24 m below the surface, similar to La Pérouse), North Pacific (Freeland,
566 1994). The difference it seems between the two seamounts concerns the average flow speed which
567 was 0.1 m s^{-1} at Cobb, compared with 0.3-0.4 m s^{-1} at La Pérouse. In other words, La Pérouse appears
568 to be in a stronger current regime preventing the formation of a Taylor column. Indeed, it should be
569 remembered that even when theoretically possible, Taylor columns can be shed from seamounts when
570 strong currents occur (White et al., 2007).

571

572 4.2. Vertical temperature structure and planktonic abundance

573 Two groups of temperature profiles were identified among the 'Flank' stations and compared with
574 'Offshore' stations. The latter, also referred to as 'control' stations, represented the typical vertical
575 temperature structure found in the western ISSG for the season (Longhurst, 1998), characterized by a
576 deep mixed layer reaching 150 m with moderate thermocline gradient. The nutricline is deep
577 associated with a distinct DCM. Group 1 of the 'Flank' stations characterized by a steady temperature
578 decrease down the water column, suggested vertical mixing at all depths (stations 3, 23 - west flank-
579 and 7 - southeast flank). In contrast, Group 2 was typified by a well stratified water column (with a
580 deep MLD) observed at stations 4, 24 (east flank) and 6 (southwest flank). Overall, the nutricline and
581 the maximum fluorescence were shallower and more intense (+30% for the fluorescence) in Group 1
582 relative to Group 2. As previously mentioned, vertical current profiles indicated a cyclonic rotation of
583 flow at stations 3 and 7, with anticyclonic motion at station 6. This suggests an upwelling-like scenario
584 at the Group 1 stations with downwelling at Group 2. More generally, this implies alternating
585 convergence and divergence flow cells sporadically around the seamount, presumably attributable to
586 the irregular shape of the seamount. These cells however, are likely to be non-permanent and will
587 evolve according to changes in current velocity and direction. Of course, this could be tested through a
588 more dense, synoptic array of measurements in future studies.

589 The zooplankton biovolume was higher on the leeward side of the seamount, particularly at
590 stations 3 and 6. However, those two stations differed in physical properties, i.e. average flow speed in
591 the upper 200 m, and vertical current patterns (high VDCI at station 3, low at station 6) belonging to
592 distinct cells (upwelling vs downwelling). Hence, no obvious physical driver is able to account for the
593 elevated biovolumes. It is possible, though, that the negative relationship between zooplankton
594 biovolume and integrated Chl *a* (upper 200 m) may suggest a top-down control by zooplankton on the
595 phytoplanktonic community through enhanced grazing especially at stations 3 and 6 (hence the lowest
596 Fmax among this group of stations) relative to the other stations around the seamount. At the
597 'Offshore' stations, no such contrast between zooplankton biovolumes and integrated Chl *a* existed,
598 suggesting that specific processes (not fully understood through our observations) may have occurred
599 in association with the seamount.

600 It is intriguing that the MODIS-Aqua data reveal only limited Chl-*a* enhancement at La Pérouse.
601 Demarcq et al. (2020) demonstrated an increase of 6-8% (relative to the average Chl-*a* in a radius of
602 90 km from the seamount) in October and during December-March around the slopes of La Pérouse.
603 Our observations showed the background chlorophyll concentration to be low, denoting overall
604 oligotrophic conditions (Fig. S4), with the small patches of chlorophyll being transient in nature (Fig.
605 S7). This does not seem unusual. Many studies carried out on seamounts do not show a consensus on
606 chlorophyll enhancement associated with seamounts. For example, significant primary production
607 enrichment was detected at the Cobb seamount (Dower et al., 1992; Comeau et al., 1995) and at
608 Komahashi N°2 seamount (Odate and Furuya, 1998), among others. However, the surveys at Great
609 Meteor Seamount (Mouriño et al., 2001) failed to demonstrate persistent increases in depth-integrated
610 primary production and biomass over the seamount. It therefore seems that seamount effects on
611 phytoplankton and zooplankton are subject to temporal and spatial variability at seasonal and shorter
612 time-scales (as shown during our experiment with regards to the evolving altimetry field). However,
613 studies by Genin and Boehlert (1985), Mohn and White (2007) among others, have shown that
614 phytoplankton enrichment tends to occur in association with cold domes and Taylor columns which
615 isolate a water mass from the surrounding areas. As mentioned earlier, elevated flow speeds prevented

the formation of any retention feature at La Pérouse, and phytoplankton enhancement might be swept away from the summit and diluted in the nearby water mass (also see Demarcq et al., 2020).

4.3. Seamount influence on micronekton

4.3.1 Micronekton distribution investigated using acoustics

The acoustic density, as a proxy of micronekton abundance, highlights clear temporal and spatial patterns around La Pérouse. The increase of the acoustic responses in the surface layer at night (87% of acoustic density) reflects the diel vertical migration of several micronekton taxa from below 400 m to the surface (top 200 m) at dusk and inversely at dawn (Lebourges-Dhaussy et al., 2000; Béhagle et al., 2014; Annasawmy et al., 2018). The intermediate layer recorded the lowest acoustic densities across all transects during both day and night because most micronekton taxa are usually vertically arranged in two well-defined surface (top 200 m) and deep (between 400 and 700 m) layers in the South West Indian Ocean (Annasawmy et al., 2020b) and only transiently occupy the intermediate zone during vertical migrations up and down the water column. The average daylight and night-time acoustic responses of the total water column recorded across the transects conducted at La Pérouse (from summit to offshore areas) were in the same range of values as recorded south of Mauritius during the Microton cruise under moderate current speeds and mesoscale variability (Annasawmy et al., 2018).

However, the micronekton acoustic densities were not distributed evenly around La Pérouse. The 'Summit and flank' area of the seamount had a lower median acoustic response compared with the 'Vicinity' and 'Offshore' areas. Low total acoustic responses over the summit of seamounts are not unusual. This was also observed at MAD-Ridge relative to 'Offshore' transects (Annasawmy et al., 2020c). The physical obstruction created by the topography has been hypothesized to explain a reduced density of deep-dweller animals over the summit and flanks of seamounts (Genin et al., 1988; Diekmann et al., 2006; De Forest and Drazen, 2009). The lower densities over the summit and slopes could also be the result of increased predation by seamount-associated predator species. Interviews carried out with recreational fishers operating at La Pérouse from 2016 to 2019, complemented by the analysis of high resolution photos provided by collaborative fishers (E.V. Romanov, unpublished),

644 sampling of demersal fish caught by bottom longline fishing on the seamount platform during the
645 cruise, and results of handline fishing experiments during the South West Indian Ocean Fisheries
646 Project (SWIOFP, World Bank) in 2008, all indicate a large diversity of benthic and pelagic predators
647 (30 species from 15 families) on the seamount. A recent inventory by a scuba diving census performed
648 in October 2019 (Durville et al., 2019) provided a new estimate of at least 120 fish species, including
649 30 predator species, with the remainder comprising small coral-associated species not sampled by
650 previous surveys. These fish predators feed primarily upon oceanic micronekton when it gathers over
651 the summit mostly during the night, and to a lesser extent, by day (Fig. 10a-b). The fish diversity at La
652 Pérouse denotes a high degree of richness when compared with other seamounts such as the East
653 Atlantic Seine Seamount, with 16 species (Christiansen et al., 2009) or the Great Meteor seamount, the
654 largest seamount in the Atlantic, with 35 species (Ehrich, 1977). On the other hand, fish diversity at La
655 Pérouse is similar to that of the Mozambique Channel seamounts (130 species; Parin et al., 2008) or
656 the Madagascar Ridge (109 species; Shcherbachev et al., 1989). However, caution must be exercised
657 when directly comparing seamount diversity, because statistical biases induced by differing sampling
658 techniques, gear and effort applied can arise.

659 Of note is that the night-time deep-trawl 2 carried out on the western side of La Pérouse (4.2 km
660 from the summit) sampled a greater proportion of fish (94%), with the seamount-associated fish
661 species *Diaphus suborbitalis* dominating the catch (Annasawmy et al., 2020b). During our cruise, this
662 species was only found close to La Pérouse both in the shallow and deep layers (Annasawmy et al.,
663 2020b; Cherel et al., 2020). Populations of *D. suborbitalis* have also been found associated with
664 continental and oceanic island slopes, mid-ocean ridges and seamounts (Kawaguchi and Shimizu,
665 1978; Bekker and Shcherbachev, 1990) such as the Equator seamount in the tropical western Indian
666 Ocean. *D. suborbitalis* prey on copepods (for small zooplankton organisms), and on other fish species
667 (e.g. *Cyclothone* sp.) and shrimps for larger individuals (Gorelova and Prut'ko, 1985). At La Pérouse,
668 *D. suborbitalis* had trophic levels ranging from 3.5 to 3.8 and were found one trophic level higher than
669 the zooplankton sampled at these stations, confirming the prey-predator relationship (Annasawmy et
670 al., 2020a).

671

672 *4.3.2 Micronekton composition investigated using trawl and stomach sampling*

673 Compared with trawl catches (Cherel et al., 2020), biological samplers (i.e. the predators) prey
674 upon fewer fish species (37 vs. 77). The dominant group in trawl catches was myctophid fish, which
675 also represented the primary prey group in top predator stomachs in the 'Open-ocean' area beyond 75
676 km from La Pérouse. The trawl samples also revealed high abundance of elongated bristlemouth fish
677 *Sigmops elongatus* (Gonostomatidae) that were absent from the stomachs of epipelagic top predators.
678 This species was caught at night in trawl hauls deeper than 100 m (Cherel et al., 2020) but was absent
679 from the daytime haul. The absence of this species in stomachs can thus be explained by its low
680 overlap with the daylight habitat of top predators, which occupy the water column higher than the
681 deep-dwelling *S. elongatus*.

682 Despite the difference in species richness between trawls and predator stomachs, the relative
683 abundance of the main dietary groups at La Pérouse shows similarities between the two sources. Fish
684 were the most abundant group (53.7% of IRI, 35.9% of trawl collections). Moreover, the second
685 dominant group in the trawls (gelatinous) was not significantly eaten by top predators. The two
686 remaining groups, crustaceans and cephalopods, were the second (28.4% of IRI; 23.7% in trawls) and
687 third (15.8%; 6.9%) most prolific taxonomic groups in the stomachs of the predators, respectively.
688 More representative samples for elusive prey such as squid are found in the predator stomachs than in
689 towed gear. This is due to the active avoidance behaviour of squid, leading to their underestimation in
690 trawls (Tsuchiya et al., 1991). The prey sampled in the stomachs (Table 6) would suggest that
691 mesopelagic fish (notably the myctophid *D. suborbitalis,* Cherel et al., 2020) and crustaceans
692 aggregate at La Pérouse.

693

694 4.4. Seamount influence on large pelagic fish and megafauna

695 Seamounts are known by fishers to attract tuna and other large pelagic fish. The importance of
696 seamounts in purse-seine and longline fisheries has also been documented and analysed extensively in
697 the Atlantic, Pacific and Indian oceans (Fonteneau, 1991; Holland and Grubbs, 2007; Morato et al.,
698 2008, 2010; Marsac et al., 2014). Processes leading to prey aggregation are often suggested to explain
699 these associations (De Forest and Drazen, 2009). The fishing maps shown in Fig. S5 fail to

demonstrate that La Pérouse is an outstanding fishing hotspot for large pelagic fish targeted by the domestic longline fleet to the west of Réunion. Rather high catches are made slightly south of the La Pérouse seamount. Nonetheless, without necessarily being a true hotspot, the two 1° squares adjacent to La Pérouse (54-55°E,19-21°S) still represent some 15% of the regional catch at the peak season. As mentioned earlier we also observe that the primary fishing area west of Réunion (54-55°E, 21-22°S) is distinguished by the presence of a deep, elongated shoal at a depth of 900 m. Among the four species targeted by the Réunion-based longline fleet, two (albacore and swordfish) are more clearly associated with this feature throughout the year (Fig. S5). Albacore is a species which exhibits a diel pattern, occupying warm waters in the mixed layer at night and deeper, cooler waters below the MLD (~ 400 to 500 m) during the day (Murray, 1994; Childers et al., 2011, Kiyofuji et al., 2013).

Stomach content studies show that albacore are opportunistic, generalist predators mostly preying on dense aggregations of pelagic fish, cephalopods and sometimes crustaceans (Williams et al., 2015). In the ISSG province, mesopelagic and meso-bathypelagic species (such as Paralepididae, Diretmiidae, Microstomatidae and others) constitute up to 23.0% of albacore stomach contents in terms of relative importance (Romanov et al., 2020). Swordfish are also deep-dwellers by day, diving as deep as 1200 m (Abecassis et al., 2012), and relying on migrating prey from the deep scatter layer during its circadian cycle. In the proximity of La Pérouse, the daylight habitat of swordfish lies between 600 and 800 m depth (Romanov et al., 2016). Mesopelagic cephalopods and fish are the main prey of swordfish in the ISSG province (Potier et al., 2007). However, swordfish also can reduce their swimming speed and feed on benthic and bentho-pelagic species at the summits of seamounts, underwater shoals and off the continental slope (Scott and Tibbo, 1968; Carey and Robison, 1981; Stillwell and Kohler, 1985). It might be then that these dietary habits and habitat utilization explain why the albacore and swordfish catch is higher west of Réunion. Moreover, it can be hypothesized that La Pérouse is perhaps too shallow (60 m) for long-term aggregation of highly mobile (horizontally and vertically) pelagic fish. Many of the seamounts cited in the literature with notable exploited tuna aggregations are deeper than La Pérouse. Examples include three seamounts off Senegal, Liberia and in the Gulf of Guinea in the Eastern Atlantic (250-350 m; Fonteneau, 1991), the Cross Seamount in the Hawaii chain (330 m; Holland and Grubbs, 2007, Gilman et al. 2012), and Travin Bank on the

Coco de Mer ridge, north of the Seychelles, in the equatorial Indian Ocean (187 m; Marsac et al., 2014), among others.

Cherel et al. (2020) report an abundance of seamount-associated myctophids around La Pérouse (*D. suborbitalis* in particular), along with hatchetfish and gonostomatids. These were identified by the use of acoustics around the seamount, and may represent a substantial food source for tuna spending large parts of their diel cycle below 300 m. However, with the exception of the myctophids recorded in predator stomachs during this study, none of the two other groups contributed significantly to the diet of albacore tuna and swordfish in the ISSG province (Romanov et al., 2020). Most of the bathy- and mesopelagic community, vulnerable to towed gears in the proximity of La Pérouse at night, in fact migrate to deeper layers at dawn, which lie outside the daylight habitat of epipelagic predators.

Steep topographies also serve as landmarks for migrating megafauna, such as cetaceans (Kaschner, 2007), sea turtles (Santos et al., 2007) and seabirds (Monteiro et al., 1996; Pinet et al., 2012) during their large-scale movements. In the case of humpback whales, the importance of underwater features was highlighted in the South Pacific (Garrigue et al., 2015), South Atlantic (Baracho-Neto et al., 2012) and South West Indian Ocean (Dulau et al., 2017). At La Pérouse, satellite tracking has revealed humpback whales using the seamount as a breeding area during the austral winter (Dulau et al., 2017). Aerial surveys conducted in the region between Mauritius and Madagascar showed the La Pérouse area broadly being used by cetacean groups (Mannocci et al., 2014). These surveys resulted in high encounter rates with marine mammals, including large delphinids, beaked whales and Globicephalinae. However, despite our cruise taking place during the humpback whale breeding season, there was no confirmed sighting of humpback whales. The only single marine mammal sighting was a pair of unidentified baleen whales. It is noteworthy that 2016 was reported as an anomalous year with very few sightings of baleen whales in the whole SWIO region (V. Dulau, pers. comm), which would explain the lack of observations in our study area.

Previous surveys undertaken in the SWIO demonstrated that Barau's petrels and wedge-tailed shearwaters occupy the southern part of the tropical Indian Ocean, in particular the Mascarene Plateau area (Le Corre et al., 2012). Brown terns, tropicbirds and noddies also frequent this area (Mannocci et al., 2014). The aerial surveys conducted in 2012 showed that the water surrounding La Pérouse is

extensively used by several seabird groups (Mannocci et al., 2014). In addition to species for which no density estimates were available, observations from their study recorded 37 brown terns per 100 km (most likely sooty terns) and 13 procellariids per 100 km (wedge-tailed and Audubon's shearwaters, Barau's petrel) around La Pérouse. However, despite a limited observational effort, seabird sightings during the La Pérouse cruise were congruent with the average estimates produced by previous surveys, highlighting the fact that La Pérouse is not a hotspot for seabirds, in terms of either diversity or foraging activity.

5. Concluding remarks

This paper presents new physical and biological data collected in the vicinity of the La Pérouse seamount in an attempt to assess whether there is a 'seamount effect' on the various trophic levels of the surrounding ecosystem. The data collected clearly showed that this steep, crescent-shaped topographic feature, located in the oligotrophic province of the Indian South Subtropical Gyre, strongly influences the circulation around the summit flanks in the upper 400 m. Consequently, it is likely that small circulation cells (convergent or divergent) are created along the slopes with implications for the vertical transport of temperature, nutrients and Chl-*a*. Certainly, satellite observations showed some Chl-*a* enrichment over the seamount. Although somewhat mismatched with Chl-*a*, these dynamics would then account for the observed spatial differences in mesozooplankton biovolume — and notably the high secondary production on the leeward (west) flank. Acoustic surveys also revealed that micronekton organisms densely aggregate in the upper layer over the summit, making them available as prey to the diverse benthic fish communities of La Pérouse, as well as migratory pelagic fish such as albacore and swordfish commonly associated with seamounts.

However in view of these encouraging observations, we could not demonstrate a sustained and remarkable biological enrichment around La Pérouse. No evidence could be found in the cruise data that suggests a Taylor column could exist there. Certainly, theoretical calculations, based on the shape of the seamount, summit depth and impinging circulation, support this finding. Moreover, and

contrary to the existing body of literature that frequently relates high productivity with seamounts, our observations suggest a far more complex and dynamic environment involving spatio-temporal variability in physical parameters across a range of scales that drive enrichment processes around seamounts. This highlights experimental design as critical for seamount studies. A full understanding of physical processes and biological responses requires synoptic and long-term measurements, repeated hydrological and acoustic transects in different directions from offshore to the seamount summit, at different seasons, and the development of high-resolution mechanistic and coupled biophysical models.

Acknowledgements

We thank the officers and crew of the R/V *Antea* for their assistance during the La Pérouse cruise, which was achieved thanks to the financial support from the Conseil Régional de La Réunion, the Flotte Océanographique Française (French Oceanographic Fleet) and the Institut de Recherche pour le Développement (IRD). We are also grateful to the UMS Imago for the logistical support provided in cruise preparation, to Pierre Rousselot for his assistance in the processing of ADCP data, and to François Baurand and Sandrine Hillion who performed the chemical analyses (nutrients and pigments) used in this paper. Finally, we thank the reviewers who improved the quality of the initial manuscript. Pavanee Annasawmy was funded through a doctoral grant provided by the IRD and the ICEMASA French-South African International Laboratory. Part of this work was supported by NE/P021050/01 - Sustainable Oceans, Livelihoods and food Security Through Increased Capacity in Ecosystem research in the Western Indian Ocean (SOLSTICE-WIO) funded by the UKRI Global Challenges Research Fund (GCRF).

References

Abecassis, M., Dewar, H., Hawn, D., Polovina, F. (2012). Modeling swordfish daytime vertical habitat in the North Pacific Ocean from pop-up archival tags. Mar Ecol Prog Ser, 452, 219-236.

Annasawmy, P., Ternon, J.F., Marsac, F., Cherel, Y., Béhagle, N., Roudaut, G., Lebourges-Dhaussy, A., Demarcq, H., Moloney, C.L., Jaquemet, S., Ménard, F. (2018). Micronekton diel migration, community composition and trophic position within two biogeochemical provinces of the South West Indian Ocean: Insight from acoustics and stable isotopes. Deep-Sea Res Part I, 138, 85–97.

Annasawmy, P., Cherel, Y., Romanov, E., Le Loc'h, F., Ménard, F., Ternon, J.F., Marsac, F. (2020a). Stable isotope patterns of mesopelagic communities over two shallow seamounts of the south-western Indian Ocean. Deep-Sea Res Part II (this issue).

Annasawmy, P., Ternon, J-F., Cotel, P., Demarcq, H., Cherel, Y, Romanov, E., Roudaut, G., Lebourges-Dhaussy, A., Ménard, F., Marsac, F. (2020b). Micronekton distribution and assemblages at two shallow seamounts in the south-western Indian Ocean: Insights from acoustics and mesopelagic trawl data. Prog Oceanogr, 178, 102161.

Annasawmy, P., Ternon, J-F., Lebourges-Dhaussy, A., Roudaut, G., Herbette, S., Ménard, F., Cotel. P., Marsac, F. (2020c). Micronekton distribution as influenced by mesoscale eddies, Madagascar shelf and shallow seamounts in the south-western Indian Ocean: An acoustic approach. Deep-Sea Res Part II (this issue).

Baracho-Neto, C.G., Neto, A.S., Rossi-Santos, M., Wedekin, L.L., Neves, M.C., Lima, F., Faria, D. (2012). Site fidelity and residence times of humpback whales (*Megaptera novaeangliae*) on the Brazilian coast. J Mar Biol Assoc UK, 92, 1783–1791.

Barruol, G., Sigloch, K. (2013). Investigating La Réunion hot spot from crust to core. EOS T Am Geophys Un, 94(23), 205-207.

Béhagle, N., Du Buisson, L., Josse, E., Lebourges-Dhaussy, A., Roudaut, G., Ménard, F. (2014). Mesoscale features and micronekton in the Mozambique Channel: an acoustic approach. Deep-Sea Res Part II, 100, 164–173.

Bekker, V.E., Shcherbachev, Y.N. (1990). Bathypelagic species of the families Neoscopelidae and Myctophidae from the Indian Ocean, with a description of a new species of *Diaphus*. J Ichthyol, 30, 122-134.

Carey, F.G., Robison, B.H. (1981). Daily patterns in the activities of swordfish, *Xiphias gladius*, observed by acoustic telemetry. Fish Bull Wash, 79(2), 277-292.

Chapman, D.C, Haidvogel, D.B (1992). Formation of Taylor caps over a tall isolated seamount in a stratified ocean. Geophys Astro Fluid, 64, 31-65.

Cherel, Y., Romanov, E., Annasawmy, P.A., Thibault, D., Ménard, F. (2020). Micronektonic fish species over three seamounts in the southwestern Indian Ocean. Deep-Sea Res Part II, https://doi.org/10.1016/j.dsr2.2020.104777

Childers, J., Snyder, S. Kohin, S. (2011). Migration and behavior of juvenile North Pacific albacore (Thunnus alalunga). Fish Oceanogr, 20, 157-173.

Chipps, S. R., Garvey, J. (2007). Quantitative assessment of food habits and feeding patterns, pp. 473–514. In: Guy C.S and Brown, M.L. (Eds) Analysis and Interpretation of Freshwater Fisheries Data. American Fisheries Society, Bethesda, MD, 971 p.

Christiansen, B., Martin, B., Hirch, S. (2009). The benthopelagic fish fauna on the summit of Seine seamount, NE Atlantic: Composition, population structure and diets. Deep-Sea Res Part II, 56(25), 2705-2712.

Clark, M.R., Schlacher, T.A., Rowden, A.A., Stocks, K.I., Consalvey, M. (2012). Science Priorities for Seamounts: Research Links to Conservation and Management. Plos One 7, e29232.

Clark, M.R., Vinnichenko, V.I., Gordon, J.D.M., Beck-Bulat, G.Z., Kukharev, N.N., Kakora, A.F. (2007). Large-scale distant-water trawl fisheries on seamounts. Chap. 17, pp 363-369. In Pitcher, T.J., Morato, T., Hart, P.J.B., Clark, M.R., Haggan, N. and Santos, R.S. (Eds) Seamounts: Ecology, Fisheries and Conservation. Fish and Aquatic Resources Series, Blackwell, Oxford, UK.

Clarke, M.R. (1986) A handbook for the identification of cephalopod beaks. Clarendon, Oxford, 286 pp.

Comeau, L.A., Vezina, A.F., Bourgeois, M., Juniper, K.S. (1995). Relationship between phytoplankton production and the physical structure of the water column near Cobb Seamount, Northeast Pacific. Deep-Sea Res Part I, 42, 993–1005.

De Forest, L., Drazen, J. (2009). The influence of a Hawaiian seamount on mesopelagic micronekton. Deep-Sea Res Part I, 56(2): 232-250.

Demarcq, H., Roberts, M.J., Noyon, M. (2020). Phytoplanktonic enhancements depicted from ocean colour remote-sensing around seamounts: examples from the south western Indian Ocean. Deep-Sea Res Part II, (this issue).

Demopoulos, A.W.J., Smith, C.R., Tyler, P.A. (2003). The Deep Indian Ocean Floor, pp 219-238. Ecosystems of the world. Elsevier.

Deplus, C., Bissessur, D., Dyment, J. (2016). Past and present volcanism around La Réunion: insights from submarine volcanic structures. RHUM-RUM workshop, La Réunion, 28 Aug-2 Sept 2016.

De Robertis, A., Higginbottom, I. (2007). A post-processing technique to estimate the signal to-noise ratio and remove echosounder background noise. ICES J Mar Sci, 64, 1282-1291.

Diekmann, R., Nellen, W., Piatkowski, U. (2006). A multivariate analysis of larval fish and paralarval cephalopod assemblages at Great Meteor Seamount. Deep-Sea Res Part I, 53, 1635-1657.

Dower, J., Freeland, H., Juniper, K., 1992. A strong biological response to oceanic flow past Cobb Seamount. Deep-Sea Res Part I, 39, 1139–1145.

Dufois, F., Hardman-Mountford, N.J., Greenwood, J., Richardson, A.J., Feng, M., Herbette, S., Matear, R. (2014). Impact of eddies on surface chlorophyll in the South Indian Ocean. J Geophys Res-Oceans, 119, 8061–8077.

Dulau, V., Pinet, P., Geyer, Y., Fayan, J., Mongin, P., Cottarel, G., Zerbini, A., Cerchio, S. (2017). Continuous movement behavior of humpback whales during the breeding season in the southwest Indian Ocean: on the road again! Mov Ecol, 5, 11.

Durville, P., Durville, S., Ballesta, L., Holon, F., Mulochau, T., Quod, J-P., Condet, M., Martigne, J-C., Trentin, F. (2019). Exploration du Mont sous-marin La Pérouse (Banc des 90 miles) au large de l'île de La Réunion. Expédition La Pérouse. Rapport de mission. Galaxea/Andromède/Vie Océane. 25 pp.

Ehrich, S., 1977. Die Fischfauna der Großen Meteorbank. Meteor Forschungsergeb- nisse, Reihe D 25, 1–23.

Fock, H.O., Matthiessen, B., Zidowitz, H., Westernhaen, H.V., (2002). Diel and habitat-dependent resource utilization by deep-sea fishes at the Great Meteor seamount: niche overlap and support for the sound scattering layer interception hypothesis. Mar Ecol Prog Ser, 244, 219-233.

Fonteneau A (1991) Monts sous-marins et thons dans l'Atlantique tropical est. Aquat Living Resour, 4, 13–25.

Freeland, H. (1994). Ocean circulation at and near Cobb seamount. Deep-Sea Res Part I, 41, 1715-1732.

Garrigue, C., Clapham, P.J., Geyer, Y., Kennedy, A.S., Zerbini, A.N. (2015). Satellite tracking reveals novel migratory patterns and the importance of seamounts for endangered South Pacific humpback whales. R Soc Open Sci, 2,150489.

Genin, A., Boehlert, G.W. (1985). Dynamics of temperature and chlorophyll structures above a seamount: an oceanic experiment. J Mar Res, 43, 907-924.

Genin, A., Haury, L., Greenblatt, P. (1988). Interactions of migrating zooplankton with shallow topography: predation by rockfishes and intensification of patchiness. Deep-Sea Res Part I, 35, 151-175.

Gilman, E., Chaloupka, M., Read, A., Dalzell, P., Holetschek, J., Curtice, C. (2012). Hawaii longline tuna fishery temporal trends in standardized catch rates and length distributions and effects on pelagic and seamount ecosystems. Aquat Conserv, 22, 446-488.

Gorelova, T. A., Prutʹko, V. G. (1985). Feeding of *Diaphus suborbitalis* (Myctophidae, Pisces) in the equatorial Indian Ocean. Oceanology-USSR, 25(4), 523-529.

Gorsky, G., Ohman, M.D., Picheral, M., Gasparini, S., Stemmann, L., Romagnan, J.B., Cawood, A., Pesant, S., García-Comas, C., Prejger, F. (2010). Digital zooplankton image analysis using the ZooScan integrated system. J Plankt Res, 32, 285–303.

Hogg, N. G. 1973. On the stratified Taylor column. J Fluid Mech, 58, 517-537.

Holland, K. N., Grubbs, R. D. (2007). Fish visitors to seamounts: Tunas and billfish at seamounts. Chap 10A, pp 189-201. In Pitcher, T.J., Morato, T., Hart, P.J.B., Clark, M.R., Haggan, N. and Santos, R.S. (Eds) Seamounts: Ecology, Fisheries and Conservation. Fish and Aquatic Resources Series, Blackwell, Oxford, UK.

Huppert, H. E. (1975). Some remarks on the initiation of internal Taylor columns. J Fluid Mech, 67, 397-412.

Huppert, H. E., Bryan, K. (1976). Topographically generated eddies. Deep-sea Res. Part I, 23: 655-679.

Ingole, B., Koslow, J.A. (2005). Deep-sea ecosystems of the Indian Ocean. Indian J Mar Sci, 34(1), 27-34.

Kaschner, K. (2007) Air-breathing visitors to seamounts: Marine Mammals. Chapt 12A. pp 230-238. In Pitcher, T.J., Morato, T., Hart, P.J.B., Clark, M.R., Haggan, N. and Santos, R.S. (Eds) Seamounts: Ecology, Fisheries and Conservation. Fish and Aquatic Resources Series, Blackwell, Oxford, UK.

Kawaguchi, K., Shimizu, H. (1978). Taxonomy and distribution of the lanternfishes, genus *Diaphus* (Pisces, Myctophidae) in the Western Pacific, Eastern Indian oceans and the Southeast Asian seas. Bull Ocean Res Inst Univ Tokyo, 10, 1-145.

Kiyofuji, H., Okamoto, S., Ijima, H. (2013). Vertical and horizontal changes of North Pacific albacore derived from archival tag data. ISC Albacore Working Group Intercessional Workshop, 5-12 November 2013, Nat. Res. Inst. Far Seas Fish., Shimizu, Shizuoka, Japan.

Lavelle, J.W., Thurnherr, A.M., Ledwell, J.R., McGillicuddy Jr., D.J., Mullineaux, L.S. (2010), Deep ocean circulation and transport where the East Pacific Rise at 9–10°N meets the Lamont seamount chain, J Geophys Res-Oceans, 115, C12073.

940 Lebourges-Dhaussy, A., Marchal., E., Menkès, C., Champalbert, G., Biessy, B. (2000). *Vinciguerria*
941 *nimbaria* (micronekton), environment and tuna: their relationships in the eastern Tropical Atlantic.
942 Oceanol Acta, 23(4), 515-528.

943 Le Bot, P., Kermabon, C., Lherminier, P. Gaillard, F. (2011). Chaine automatisée de suivi des
944 courantomètres acoustiques Doppler embarqués. Cascade V6.1 : logiciel de validation et de
945 visualisation des mesures ADCP de coque. Rapport OPS/LPO 11-01, Ifremer, France, 93 p.

946 Le Corre, M., Jaeger, A., Pinet, P., Kappes, M.A., Weimerskirch, H., Catry, T., Ramos, J.A., Russell,
947 J.C., Shah, N., Jaquemet, S. (2012). Tracking seabirds to identify potential Marine Protected Areas
948 in the tropical western Indian Ocean. Biol Conserv, 83–93.

949 Longhurst, A.R. (1998). Ecological geography of the sea. Academic Press, 398 pp.

950 Lu, C.C., Ickeringill, R. (2002). Cephalopod beak identification and biomass estimation techniques:
951 tools for dietary studies of southern Australian finfishes. Mus Victoria Sci Rep, 6, 1-65.

952 Mannocci, L., Laran, S., Monestiez, P., Dorémus, G., Van Canneyt, O., Watremez, P., Ridoux, V.
953 (2014). Predicting top predator habitats in the Southwest Indian Ocean. Ecography, 37, 261–278.

954 Marsac, F., Fonteneau, A., Michaud, P. (2014). Le coco de mer, une montagne sous la mer, Chap 7,
955 pp. 151-163. In : Marsac, F., Fonteneau, A. and Michaud, P., L'or bleu des Seychelles: histoire de
956 la pêche industrielle au thon dans l'océan Indien. IRD Editions, 269 pp.

957 Mohn, C., White, M. (2007). Remote sensing and modelling of bio-physical distribution patterns at
958 Porcupine and Rockall Bank, Northeast Atlantic. Cont Shelf Res, 27, 1875-1892.

959 Mohn, C., White, M., Bashmachnikov, I., Jose, F., Pelegri, J.L. (2009). Dynamics at an elongated,
960 intermediate depth seamount in the North Atlantic (Sedlo Seamount, 40°20'N, 26°40'W). Deep-
961 Sea Res Part II, 56, 2582–2592.

962 Monteiro, L.R., Ramos, J.R., Furness, R.W., del Nevo, A.J. (1996). Movements, morphology,
963 breeding, molt diet and feeding of seabirds in the Azores. Colon Waterbird, 19, 82–97.

964 Morato, T., Clark, M.R. (2007). Seamount fishes: ecology and life histories. Chapt 9, pp 170-188. In
965 Pitcher, T.J., Morato, T., Hart, P.J.B., Clark, M.R., Haggan, N. and Santos, R.S. (Eds) Seamounts:
966 Ecology, Fisheries and Conservation. Fish and Aquatic Resources Series, Blackwell, Oxford, UK.

967 Morato, T., Hoyle, S.D., Allain, V., Nicol, S.J. (2010). Tuna longline fishing around West and Central
968 Pacific seamounts. Plos One, 5(12), e14453.

969 Morato, T., Varkey, D. A., Damaso, C., Machete, M., Santos, M., Prieto, A., Santos, R.S., Pitcher, T.
970 (2008). Evidence of a seamount effect on aggregating visitors. Mar Ecol Prog Ser, 357, 23-32.

971 Mouriño, B., Fernandez, E., Serret, P., Harbour, D., Sinha, B., Pingree, R. (2001). Variability and
972 seasonality of physical and biological fields at the Great Meteor Tablemount (subtropical NE
973 Atlantic). Oceanol Acta, 24(2), 167-185.

974 Murray, T. (1994). A review of the biology and fisheries for albacore, *Thunnus alalunga*, in the South
975 Pacific Ocean, pp 188-206. In: Shomura, R.S., Majkowski, J. and Langi, S. (Eds) Interaction of
976 Pacific tuna fisheries. FAO Fish. Tech. Pap., 336(2), 439 p.

977 Noyon, M., Rasoloarijao, Z., Huggett, J., Ternon, J-F., Roberts, M.J. (2020). Comparison of
978 mesozooplankton communities at three shallow seamounts in the South West Indian Ocean. Deep-
979 Sea Res Part II, this issue, https://doi.org/10.1016/j.dsr2.2020.104759

980 Odate, T., Furuya, K. (1998). Well-developed subsurface chlorophyll maximum near Komahashi No.
981 2 Seamount in the summer of 1991. Deep-Sea Res Part I, 45, 1595–1607.

982 Parin, N. V., Timokhin, I. G., Novikov, N. P., Shcherbachev, Y. N. (2008). On the composition of
983 talassobathyal ichthyofauna and commercial productivity of Mozambique Seamount (the Indian
984 Ocean). J Ichthyol, 48(5), 361–366.

985 Perrot Y., Brehmer P., Habasque J., Roudaut G., Béhagle N., Sarre A., Lebourges-Dhaussy A. (2018).
986 Matecho: an open-source tool for processing fisheries acoustics data. Acoust Aust, 46(2), 241-248.

987 Picheral, M., Colin, S., Irisson, J-O. (2017). EcoTaxa, a tool for the taxonomic classification of
988 images. URL http://ecotaxa.obs-vlfr.fr

989 Pinet, P., Jaquemet, S., Phillips, R.A., Le Corre, M. (2012). Sex-specific foraging strategies
990 throughout the breeding season in a tropical, sexually monomorphic small petrel. Anim Behav, 83,
991 979-989.

992 Pinkas, L., Oliphant, M.S., Iverson, I.L.K. (1971). Food habits of albacore, bluefin tuna, and bonito in
993 California waters. Fish Bull US, 152, 1-105.

994 Pitcher, T.J., Bulman, C. (2007). Raiding the larder: a quantitative evaluation framework and trophic
995 signature for seamount food webs. Chapt 14, pp 282-295. In Pitcher, T.J., Morato, T., Hart, P.J.B.,
996 Clark, M.R., Haggan, N. and Santos, R.S. (Eds) Seamounts: Ecology, Fisheries and Conservation.
997 Fish and Aquatic Resources Series, Blackwell, Oxford, UK.

998 Potier, M., Marsac, F., Cherel, Y., Lucas, V., Sabatie, R., Maury, O., Ménard, F. (2007). Forage fauna
999 in the diet of three large pelagic fish (lancetfish, swordfish and yellowfin tuna) in the western
1000 equatorial Indian Ocean. Fish Res, 83, 60-72.

1001 Potier, M., Ménard, F., Benivary, H. D., Sabatié, R. (2011). Length and weight estimates from
1002 diagnostic hard part structures of fish, crustacea and cephalopods forage species in the western
1003 Indian Ocean. Environ Biol Fish, 92, 413–423.

1004 Roberts, M.J., Ternon, J-F., Marsac, F., Noyon, M. (2020). The MADRidge Project : Bio-physical
1005 coupling around three shallow seamounts in the South Western Indian Ocean. Deep-Sea Res Part II
1006 (this issue).

1007 Rogers, A.D., Clark, M.R., Hall-Spencer, J.M., Gjerde, K.M. (2008). The science behind the
1008 guidelines: a scientific guide to the FAO draft international guidelines (December 2007) for the
1009 management of deep-sea fisheries in the High Seas and examples of how the guidelines may be
1010 practically implemented. IUCN, Switzerland.

1011 Romanov, E.V. (2003). Summary and review of Soviet and Ukrainian scientific and commercial
1012 fishing operations on the deepwater ridges of the southern Indian Ocean. FAO Fisheries Circular.
1013 No. 991. FAO, Rome, 84 pp.

1014 Romanov, E., Sabarros, P.S., Le Foulgoc, L., Bach, P. (2016). A preliminary analysis of swordfish
1015 (*Xiphias gladius*) habitat and behaviour on migratory track from Reunion Island to equatorial
1016 waters. IOTC Working Party on Billfish (WPB) Victoria, Seychelles, 06-10 September 2016.
1017 IOTC–2016–WPB14–16. 20 p.

1018 Romanov, E.V., Nikolic, N., Dhurmeea, Z., Bodin, N., Puech, A., Norman, S., Hollanda, S., Bourjea,
1019 J., West W., Potier M. (2020). Trophic ecology of albacore tuna *Thunnus alalunga* in the western
1020 tropical Indian Ocean and adjacent waters. Mar Fresh Res, in press.

1021 Ryan, T.E., Downie, R.A., Kloser, R.J., Keith, G. (2015). Reducing bias due to noise and attenuation
1022 in open-ocean echo integration data. ICES J Mar Sci, 72, 2482-2493.

1023 Santos, M.A., Bolton, A.B., Martins, H.R., Riewald, B., Bjorndal, K.A. (2007). Air-breathing visitors
1024 to seamounts: sea turtles. Chapt 12B, pp 239-244. In Pitcher, T.J., Morato, T., Hart, P.J.B., Clark,
1025 M.R., Haggan, N. and Santos, R.S. (Eds) Seamounts: Ecology, Fisheries and Conservation. Fish
1026 and Aquatic Resources Series, Blackwell, Oxford, UK.

1027 Shcherbachev, A. N. Kotlyar, Abramov, A.A (1989). Ichthyofauna and Fish Stock of Seamounts of
1028 the Indian Ocean, pp 159-185. In: Biological Resources of the Indian Ocean (Nauka, Moscow).

1029 Scott, W.B., Tibbo, S.N. (1968). Food and feeding habits of swordfish, *Xiphias gladius*, in the western
1030 North Atlantic. J Fish Res Board Can, 25, 903-919.

1031 Smale, M.J., Watson, G, Hecht, T. (1995). Otolith Atlas of southern African marine fishes.
1032 Ichthyological Monographs, 1. J.L.B. Smith Institute of Ichthyology, Grahamstown, 420 pp.

1033 Stillwell, C.E., Kohler, N.E. (1985). Food and feeding ecology of the swordfish *Xiphias gladius* in the
1034 western North Atlantic Ocean with estimates of daily ration. Mar Ecol Prog Ser, 22, 239-247.

1035 Sprintall, J., Cronin, M.F. (2009). Upper ocean vertical structure, pp 217-224. Encyclopedia of Ocean
1036 Sciences (Second Edition), Academic Press, 3900 p.

1037 Taylor, G. I. (1923). Experiments on the motion of solid bodies in rotating fluids. Proc R Soc. A, 104,
1038 213-218.

1039 Tomczak, M., Godfrey, J.S. (1994). The Indian Ocean. In: Regional Oceanography: An Introduction.
1040 Elsevier, UK, 391 p.

1041 Trenkel, V.M., Berger, L., Bourguignon, S., Doray, M., Fablet, R., Massé, J., Mazauric, V., Poncelet,
1042 C., Quemener, G., Scalabrin, C., Villalobos, H. (2009). Overview of recent progress in fisheries
1043 acoustics made by Ifremer with examples from the Bay of Biscay. Aquat Living Resour, 22, 433-
1044 445.

1045 Tsuchiya, K., Piatkowski, U., Okutani, T. (1991). Distribution and re-description of *Abraliopsis*
1046 *lineata* Goodrich, 1896 (Cephalopoda, Enoploteuthidae) from the Arabian Sea. J Nat Hist, 25(5),
1047 1121–1133.

1048 Vandromme, P., Lars, S., García-Comas, C., Berline, L., Sun, X., Gorsky, G. (2012). Assessing biases
1049 in computing size spectra of automatically classified zooplankton from imaging systems: A case
1050 study with the ZooScan integrated system. Meth Oceanogr. 1–2, 3–21.

1051 Visbeck M. (2001). Deep velocity profiling using lowered acoustic Doppler current profilers: bottom-
1052 track and inverse solutions. J Atmos Ocean Tech, 19, 794-807.

1053 White, M., Bashmachnikov, I., Arístegui, J., Martins, A. (2007) Physical processes and seamount
1054 productivity. Chapter 4., pp 65-84. In Pitcher, T.J., Morato, T., Hart, P.J.B., Clark, M.R., Haggan,
1055 N. and Santos, R.S. (Eds) Seamounts: Ecology, Fisheries and Conservation. Fish and Aquatic
1056 Resources Series, Blackwell, Oxford, UK.

1057 Williams, A.J., Allain, V., Nicol, S.J., Evans, K.J., Hoyle, S.D., Dupoux, C., Vourey, E., Dubosc, J.
1058 (2015). Vertical behavior and diet of albacore tuna (*Thunnus alalunga*) vary with latitude in the
1059 South Pacific Ocean. Deep-Sea Res Part II, 113, 154-169.

List of figures

Figure 1. Location of the La Pérouse seamount on a regional map. Red diamond symbols indicate stomach samples associated with La Pérouse seamount. Blue circles denote the open-ocean samples. (a); 3-D view of the seamount showing the crescent-shaped summit (b); high resolution bathymetric map of La Pérouse and immediate surroundings, measured during the Antea-Pérouse cruise, 15-29 September 2016 (c), showing the location of 11 hydrological stations and zooplankton tows (red diamonds), and 10 midwater trawl hauls (blue lines).

Figure 2. Sea level anomalies on 19 September (a) and 3 October 2016 (b) with overlaid geostrophic currents (red arrows) deduced from satellite altimetry. The velocity scale of the arrows is indicated in the legend. Cyclonic eddies are represented with dashed contours. Anticyclonic eddies with solid lines. Stations at La Pérouse are represented by blue triangles.

Figure 3. Vertical sections for S-ADCP total velocity from Réunion to La Pérouse, 16-18 September 2016 (a) and from La Pérouse to Réunion, 28-29 September 2016 (b).

Figure 4. Box and whisker plots for current velocity determined by the L-ADCP, in the upper 200 m (a) and upper 400 m (b) for both the 'Offshore' (control) and the "Flank" stations.

Figure 5. Grouped vertical temperature (left panels, a-c) and chlorophyll-a (right panels, d-f) profiles (1 = Offshore; 2-3 = Flank). The dotted lines indicate the MLD in the left panels and the depth of the nutricline in the right panels for each station

Figure 6. Spatial distribution of zooplankton biovolume at 10 stations (summit station 5 not sampled). Note the relatively high biovolume at station 7 is biased by the presence of a single large-size Trachymedusa not recorded in any of the other Bongo net samples.

Figure 7. Zooplankton biovolume as a function of the integrated Chl-*a* in the upper 200 m. Numbers indicate the stations where Bongo nets tows were deployed. 'Flank' stations are denoted by grey circles and 'Offshore' stations by triangles. The linear fit is shown for the 'Flank' stations only.

1085 **Figure 8**. Location of acoustic transects in the 'Vicinity' and 'Offshore' zones (day= yellow; night=
1086 cyan) and on the 'Summit and flank' of La Pérouse (day= red; night= blue) (a). Micronekton average
1087 acoustic density (NASC, m^2 nmi^{-2}) by transect during the day (b) and at night (c).

1088 **Figure 9**. Box and whisker plot for the overall micronekton acoustic densities, in the day and at night,
1089 for the aforementioned groups of acoustic transects in Fig. 12a.

1090 **Figure 10**. Typical echograms recorded on the flanks and summit of La Pérouse during daylight (a)
1091 and at night (b).

1092

1093 Table 1 – Summary of hydrological stations. Note that local time during the cruise is GMT+3. Stations
1094 are categorized as offshore (O) or flank (F) based on the distance to the seamount (70 m depth
1095 contour).

Station	Date	Local time	Latitude	Longitude	Dist. to seamount (km)	Position attribute
1	21/09/2016	11:09:58	19°32.69' S	54°11.95' E	14.4	O
2	22/09/2016	12:53:29	19°49.58' S	54°05.93' E	9.9	O
3	23/09/2016	06:24:18	19°40.06' S	54°09.09' E	1.5	F
4	23/09/2016	09:13:42	19°42.02' S	54°11.29' E	1.3	F
5	23/09/2016	12:29:08	19°43.67' S	54°09.70' E	1.1	F
6	23/09/2016	13:39:31	19°44.95' S	54°06.30' E	3.2	F
7	23/09/2016	17:52:30	19°46.34' S	54°09.38' E	2.2	F
8	25/09/2016	06:15:47	19°42.55' S	53°56.55' E	21.1	O
10	26/09/2016	06:22:31	19°42.59' S	54°20.02' E	20	O
23	27/09/2016	11:35:11	19°41.90' S	54°06.50' E	2.2	F
24	27/09/2016	18:23:10	19°44.76' S	54°11.06' E	1.1	F

1096

1097 Table 2 – Summary of trawl stations at La Pérouse and shortest distance to the seamount (70 m depth
1098 contour). Position attributes: S=Summit, V=Vicinity, F=Flank, O=Offshore

Trawl #	Latitude	Longitude	Max trawl depth (m)	Distance (km)	Position attribute	Start/end local time	Day/ Night	Trawling speed (knots)
1	19° 43'S	54° 04'E	590	6.00	V	17:10 18:55	N	3.0
2	19° 44'S	54° 06'E	400	4.20	V	17:20 18:55	N	3.2
3	19° 39'S	53° 52'E	90	28.4	O	18:30 20:00	N	2.7
4	19° 39'S	54° 10'E	110	4.00	V	18:15 19:45	N	3.0
5	19° 44'S	54° 09'E	35	0	S	08:33 09:35	D	3.6
6	19° 42'S	54° 12'E	60	1.15	F	18:44 19:54	N	3.0
7	19° 36'S	54° 08'E	500	7.70	V	17:59 19:50	N	3.0
8	19° 48'S	54° 07'E	430	6.45	V	16:21 18:30	N	3.2
9	19° 49'S	54° 07'E	240	6.76	V	19:05 20:37	N	3.2
10	19° 45'S	54° 15'E	250	7.60	V	19:25 21:10	N	4.0

1099

1100 Table 3 – Summary statistics of stomachs sampled from six different top predator species

Predators	La Pérouse vicinity		Open-ocean	
	3-10 km		75-280 km	
	n	size range (cm)	n	size range (cm)
Thunnus alalunga	5	95-106	31	88-111
Thunnus albacares			3	71-157
Thunnus obesus			5	76-154
Xiphias gladius			9	122-191
Coryphaena hippurus	3	80-98	2	94-100
Alepisaurus ferox	4	77-123	16	56-145
	12		**81**	

1101

Table 4 – Spatial stratification by distance to the seamount summit used in this study, across the different data sets. The numbers indicate the number of samples, except for acoustic data where the cumulative transect lengths is given (km). The trawl data are not included in this stratification scheme because not used for the spatial analysis, neither fisheries data as a 1°grid was applied for the entire South West Indian Ocean. Acoustic data were not discriminated between summit and flank.

Data sets		**Summit**	**Flank**	**Vicinity**	**Offshore**	**Open-ocean**
			0 to 3 km	3 to 10 km	10 to 35 km	75-280 km
Hydrological stations			7		4	
Bongo nets			6		4	
Acoustic surveys	Day	95 km		162 km		
	Night	29 km		110 km	123 km	
Stomachs				12		81

Table 5– Vertical Directional Change Index (VDCI) and deviation to the mean (specific to each group) by station and location ('Offshore' vs 'Flank') for two depth ranges. The highest two VDCI values are indicated in bold.

			Range 0-200 m		Range 0-400 m	
Location	Station no	Bottom depth (m)	VDCI	Deviation to the mean	VDCI	Deviation to the mean
Offshore	1	3968	75	-63	576	+36
	2	2386	74	-63	317	-223
	8	4203	108	-29	512	-28
	10	1654	291	+154	754	+215
Flank	3	1254	**630**	+208	**1255**	+412
	23	1260	152	-272	**914**	+71
	6	1105	240	-182	517	-326
	7	1400	473	+50	814	-29
	24	895	483	+61	835	-8
	5	200	**686**	+264	-	-
	4	550	294	-129	722	-121

Table 6 – The percentage composition of prey items found in top predator stomachs, expressed as the index of relative importance (IRI) and mean reconstituted weight (MRW) of each large taxonomic group

	La Pérouse vicinity		Open-ocean	
	%IRI	%MRW	%IRI	%MRW
Cephalopods	15.8	41.8	40.3	41.5
Other molluscs	2.1	0.2	3.0	1.4
Crustaceans	28.4	19.7	11.9	4.0
Fish	53.7	38.3	44.6	53.1
Other prey, incl. plastic	0	0	0.1	<0.1

1118

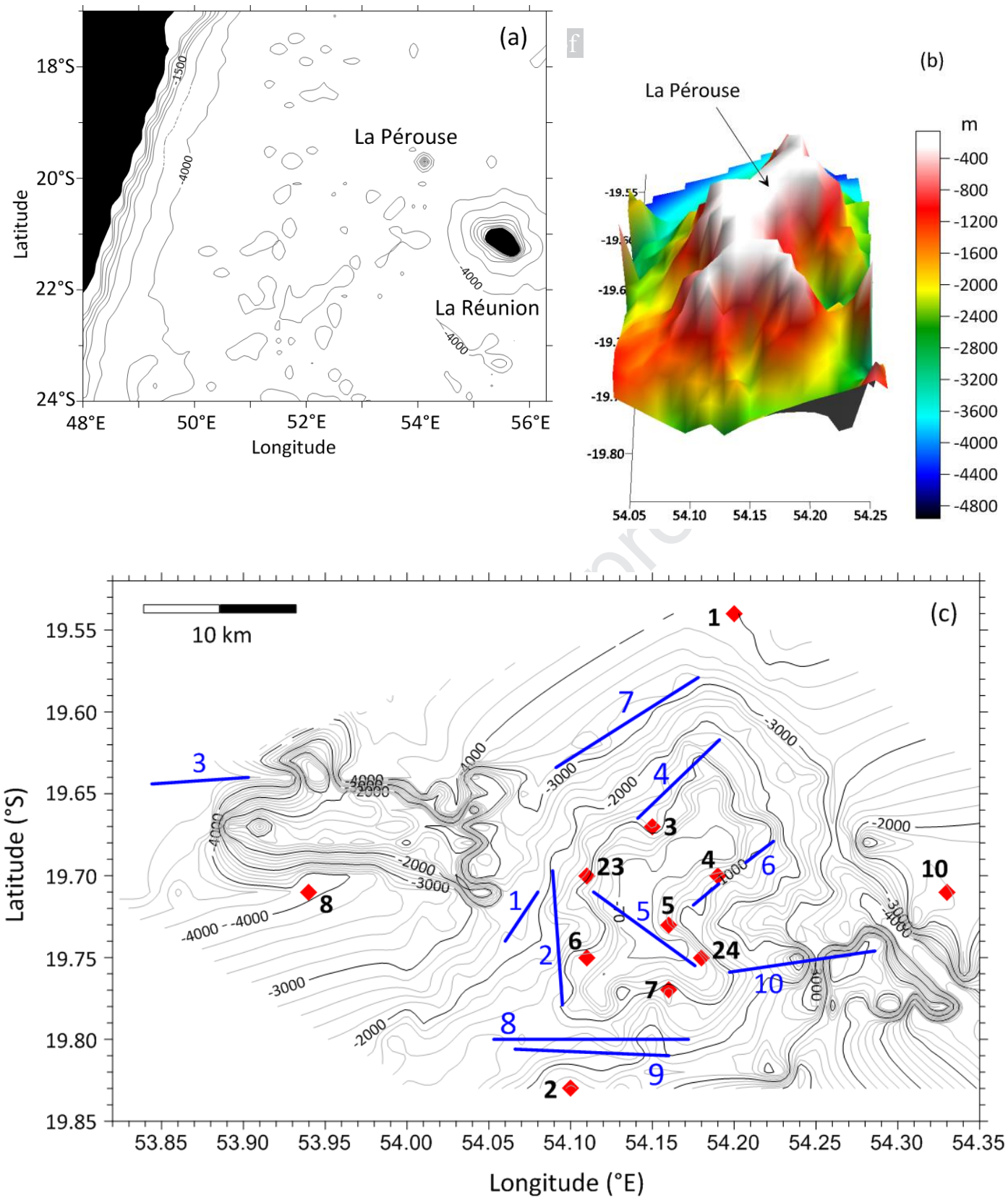
(a)
La Pérouse
La Réunion
Latitude
Longitude
18°S
20°S
22°S
24°S
48°E
50°E
52°E
54°E
56°E
-1500
-4000
(b)
La Pérouse
m
-400
-800
-1200
-1600
-2000
-2400
-2800
-3200
-3600
-4000
-4400
-4800
54.05
54.10
54.15
54.20
54.25
-19.80
(c)
10 km
Latitude (°S)
Longitude (°E)
19.55
19.60
19.65
19.70
19.75
19.80
19.85
53.85
53.90
53.95
54.00
54.05
54.10
54.15
54.20
54.25
54.30
54.35
-2000
-3000
-4000
1
2
3
4
5
6
7
8
9
10
23
24

Figure 1

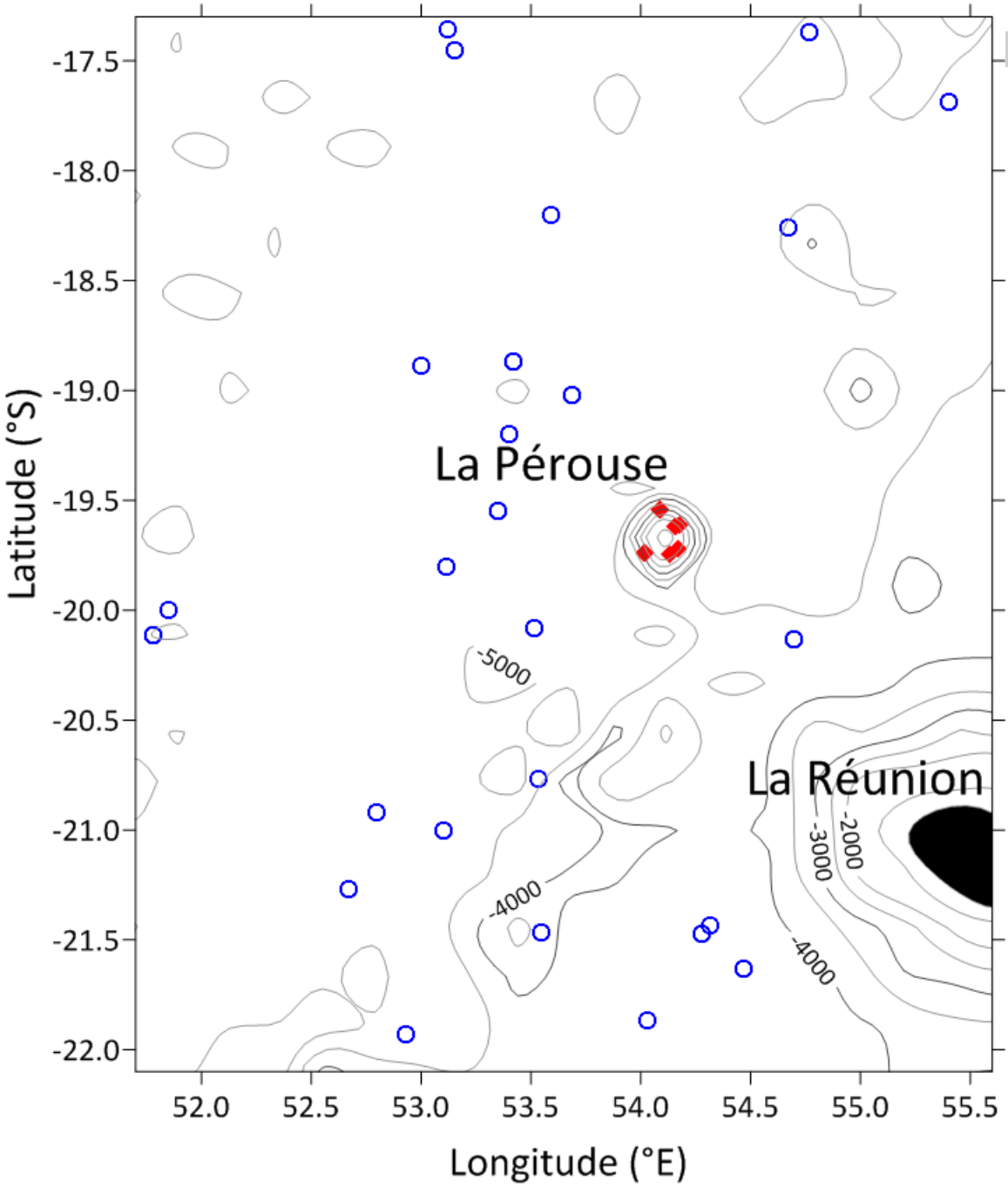
-17.5
-18.0
-18.5
-19.0
-19.5
-20.0
-20.5
-21.0
-21.5
-22.0
Latitude (°S)
52.0
52.5
53.0
53.5
54.0
54.5
55.0
55.5
Longitude (°E)
La Pérouse
La Réunion
-5000
-4000
-3000
-2000
-4000

Figure 2

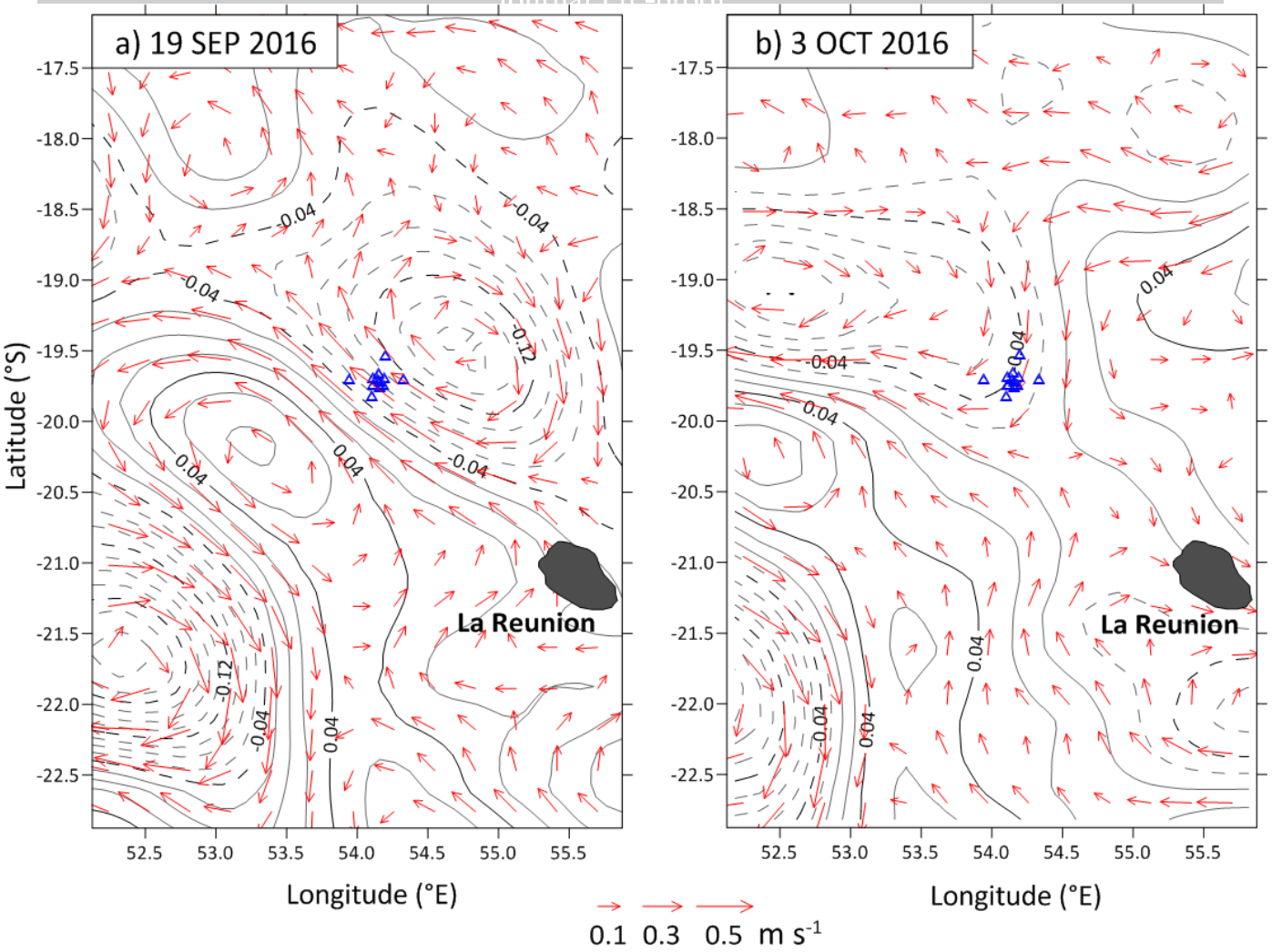

Figure 3

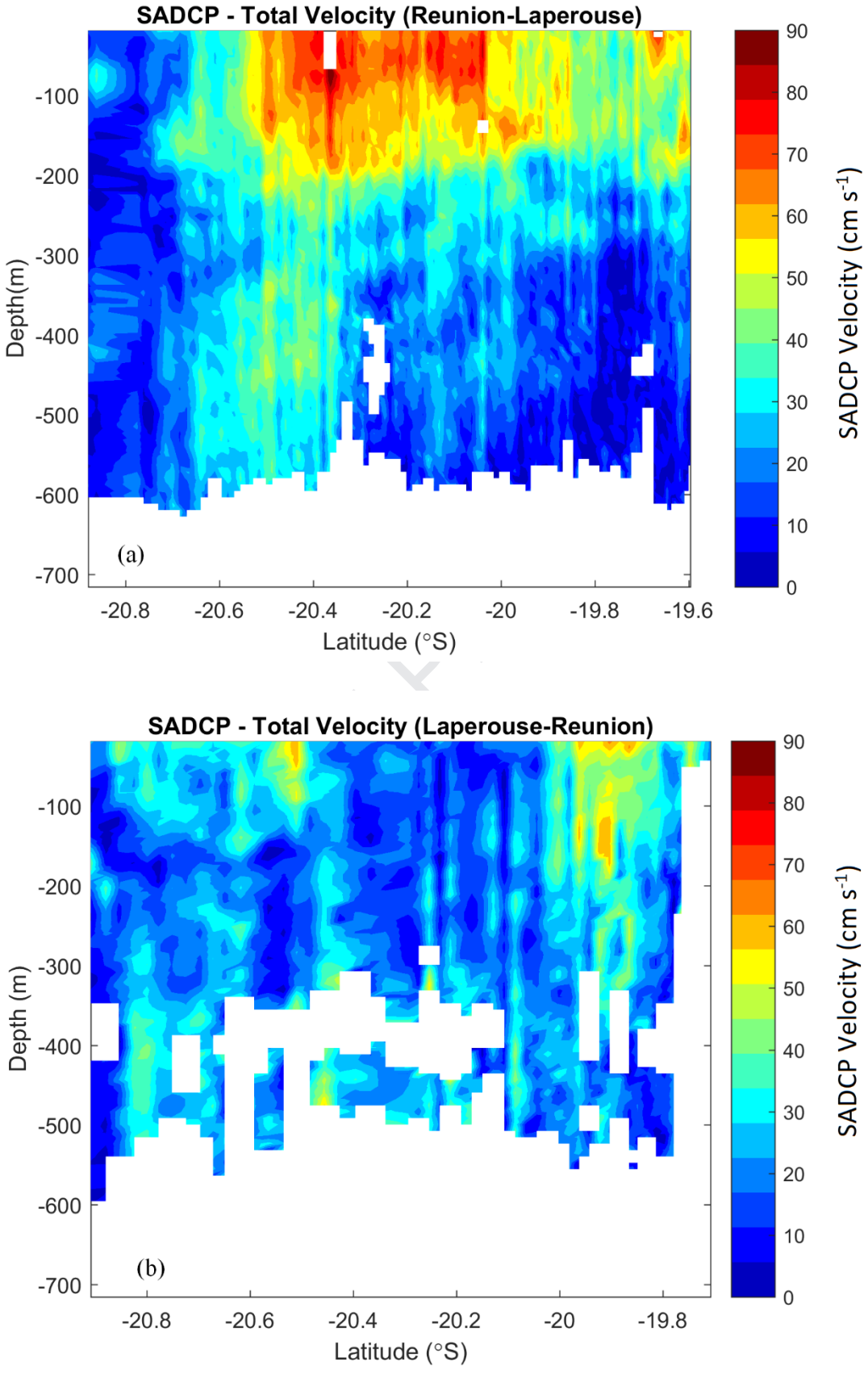
SADCP - Total Velocity (Reunion-Laperouse)
Depth(m)
-100
-200
-300
-400
-500
-600
-700
(a)
-20.8
-20.6
-20.4
-20.2
-20
-19.8
-19.6
Latitude (°S)
90
80
70
60
50
40
30
20
10
0
SADCP Velocity (cm s-1)
SADCP - Total Velocity (Laperouse-Reunion)
Depth (m)
-100
-200
-300
-400
-500
-600
-700
(b)
-20.8
-20.6
-20.4
-20.2
-20
-19.8
Latitude (°S)
90
80
70
60
50
40
30
20
10
0
SADCP Velocity (cm s-1)

Figure 4

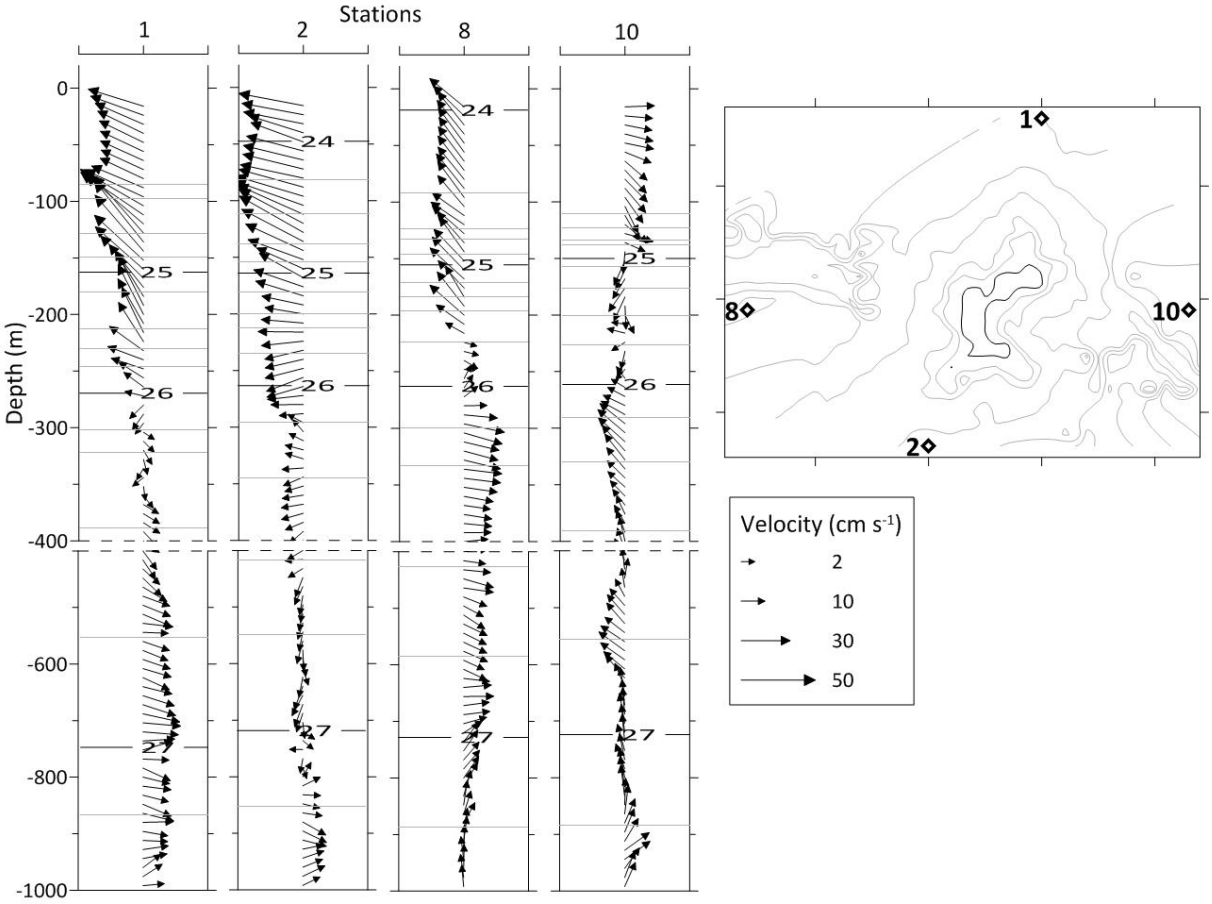

Figure 5

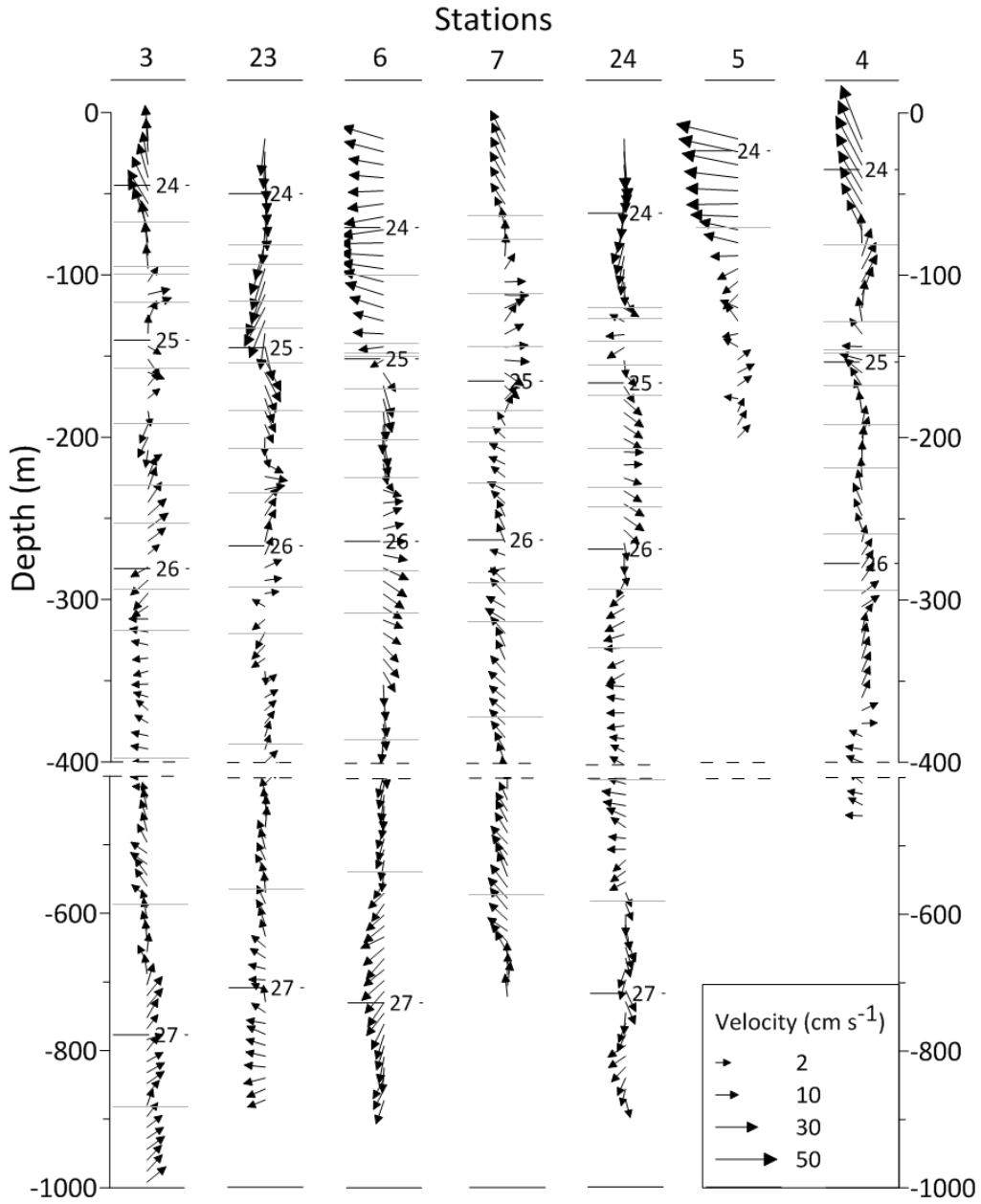
Stations
3
23
6
7
24
5
4
Depth (m)
0
-100
-200
-300
-400
-600
-800
-1000
24
25
26
27
Velocity (cm s-1)
2
10
30
50

Figure 6

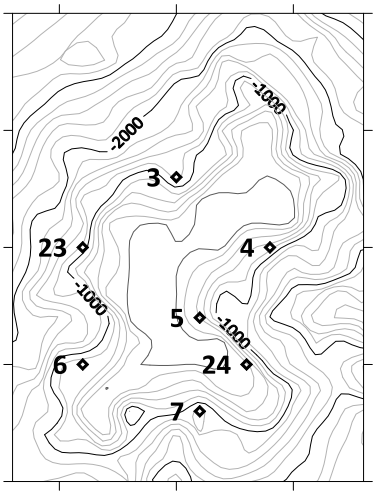
-1000
-2000
3
23
4
5
6
24
7

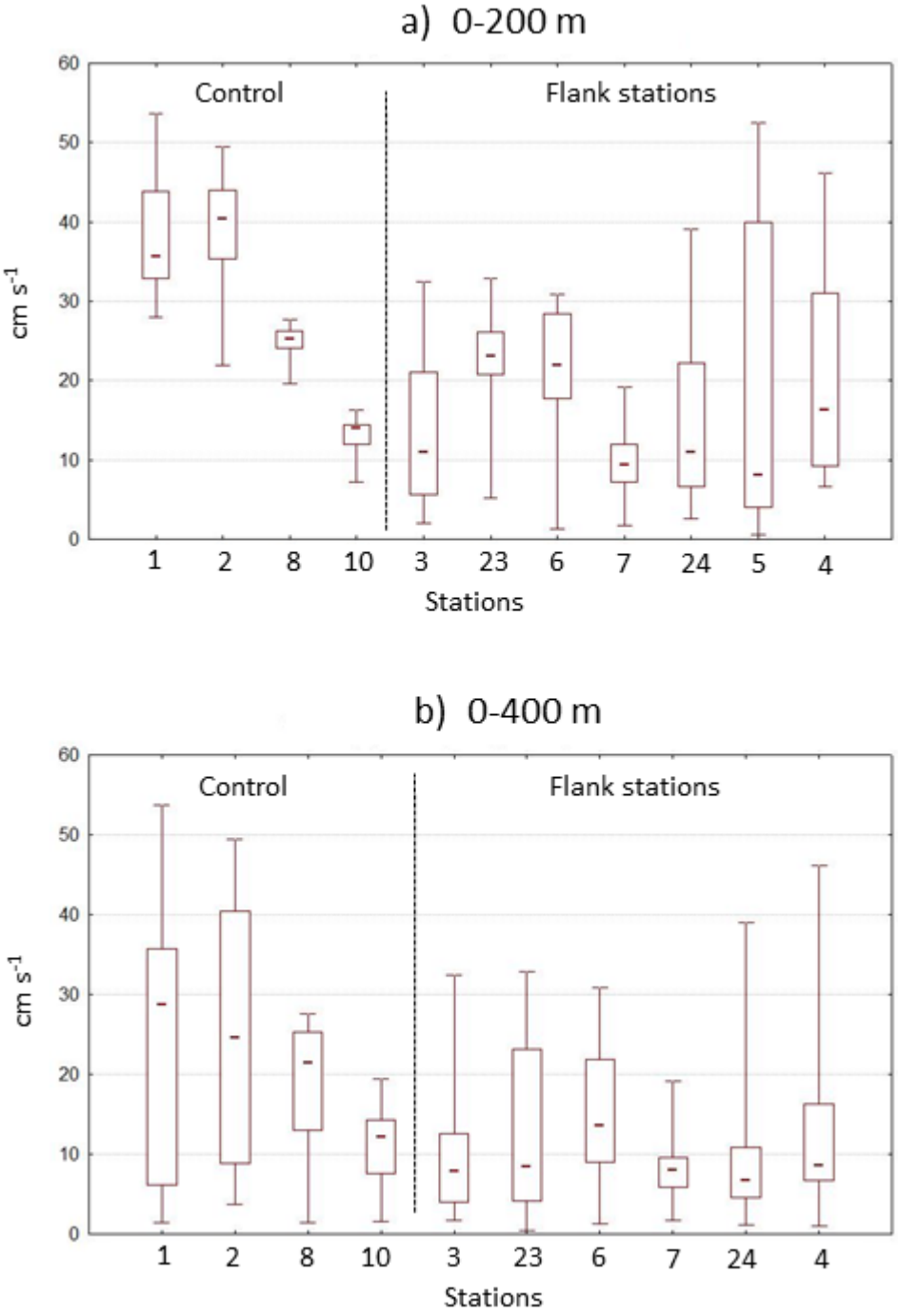
a) 0-200 m
Control
Flank stations
cm s-1
0
10
20
30
40
50
60
1
2
8
10
3
23
6
7
24
5
4
Stations
b) 0-400 m
Control
Flank stations
cm s-1
0
10
20
30
40
50
60
1
2
8
10
3
23
6
7
24
4
Stations

Figure 7

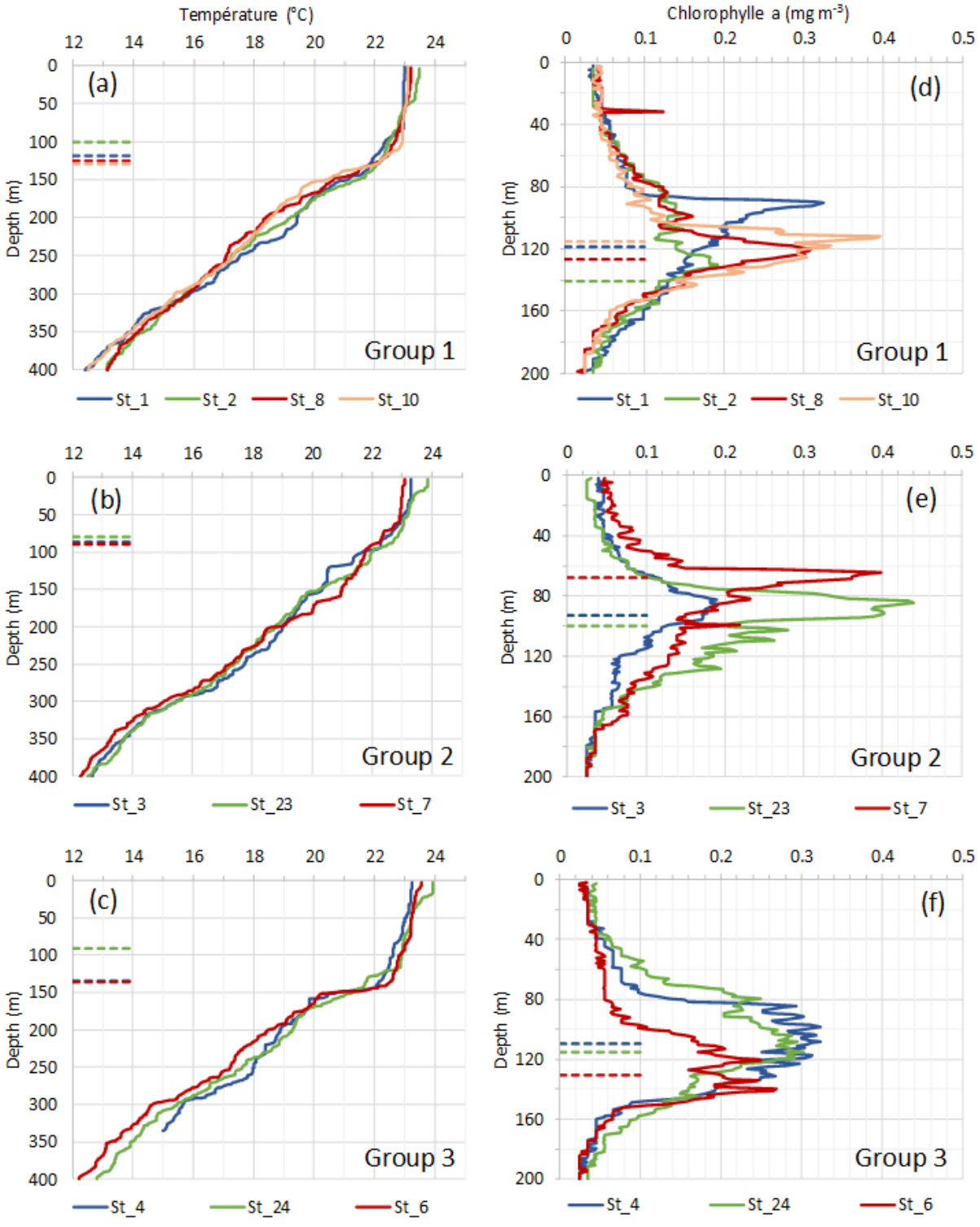
Température (°C)
Chlorophylle a (mg m-3)
(a)
(b)
(c)
(d)
(e)
(f)
Depth (m)
Group 1
Group 2
Group 3
St_1
St_2
St_8
St_10
St_3
St_23
St_7
St_4
St_24
St_6

Figure 8

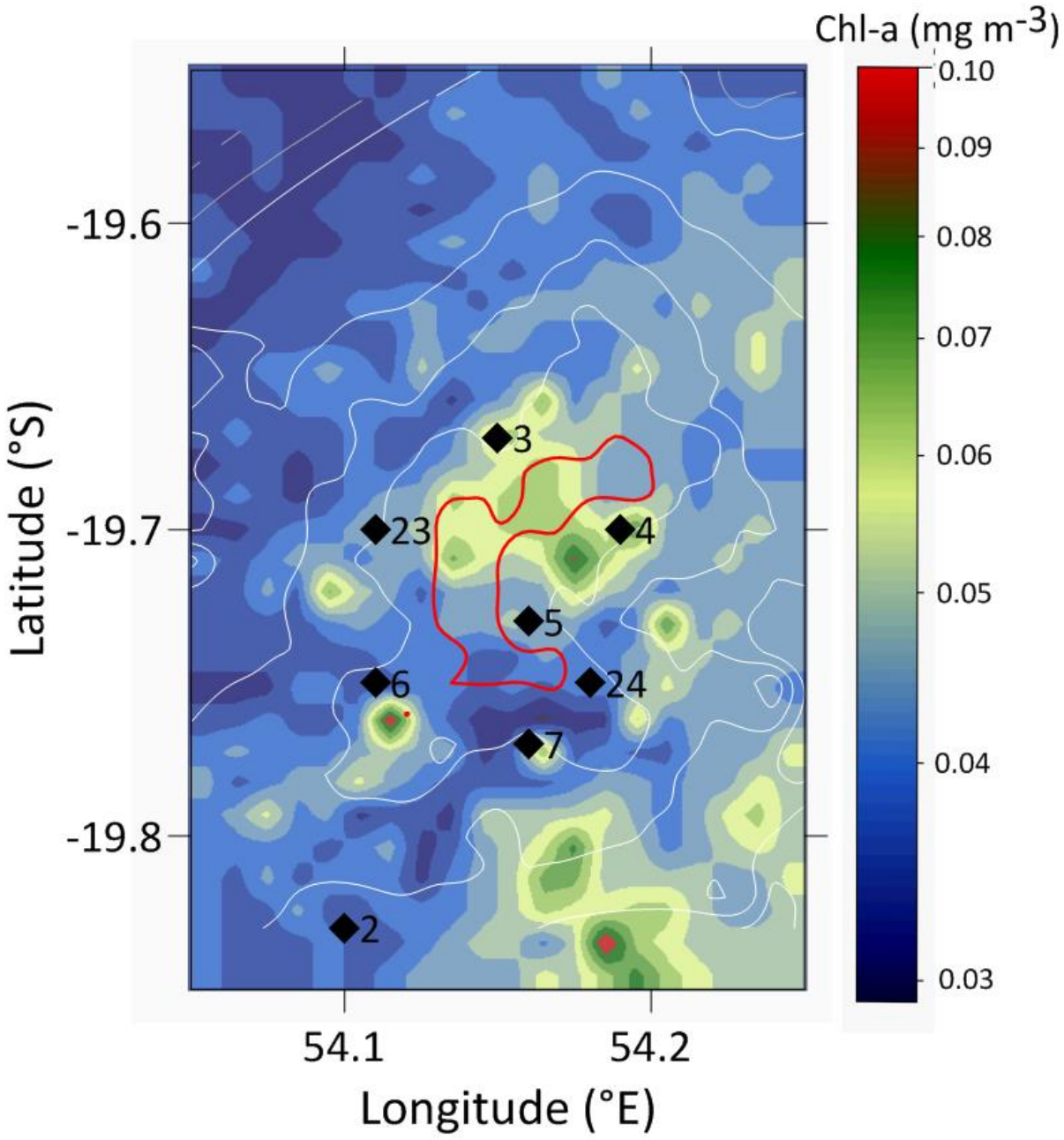
Chl-a (mg m-3)
0.10
0.09
0.08
0.07
0.06
0.05
0.04
0.03
-19.6
-19.7
-19.8
Latitude (°S)
54.1
54.2
Longitude (°E)
3
23
4
5
6
24
7
2

Fig. 9

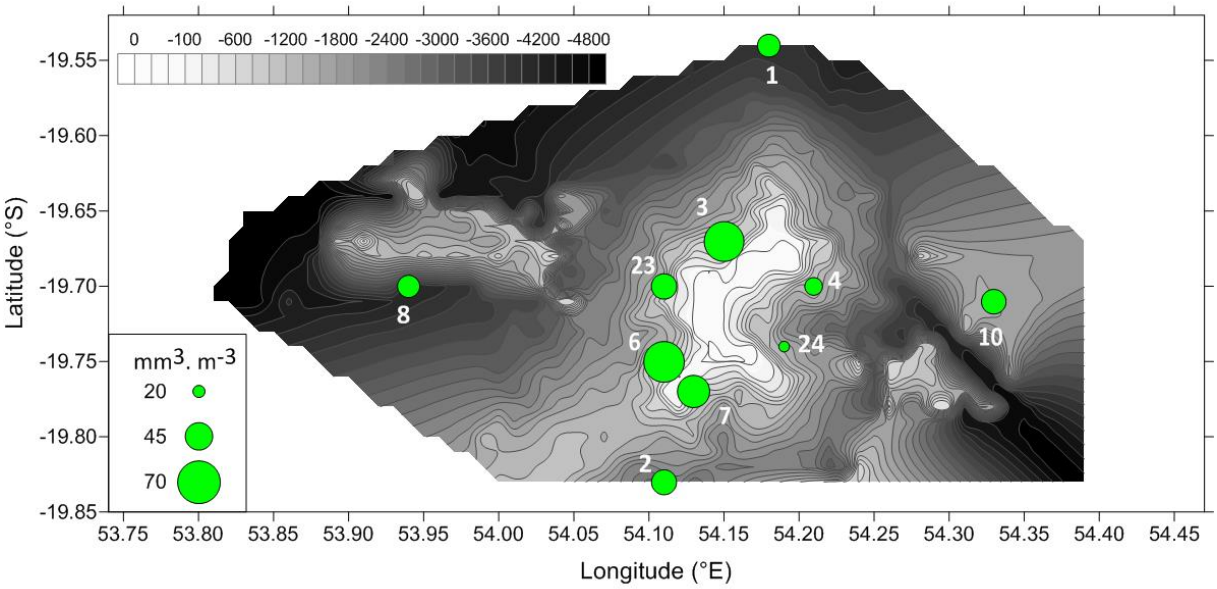

Figure 10

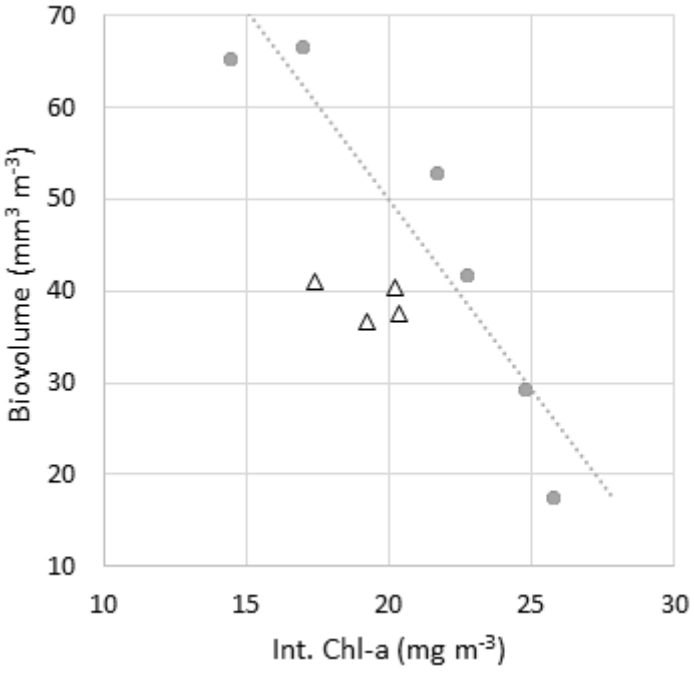

Figure 11

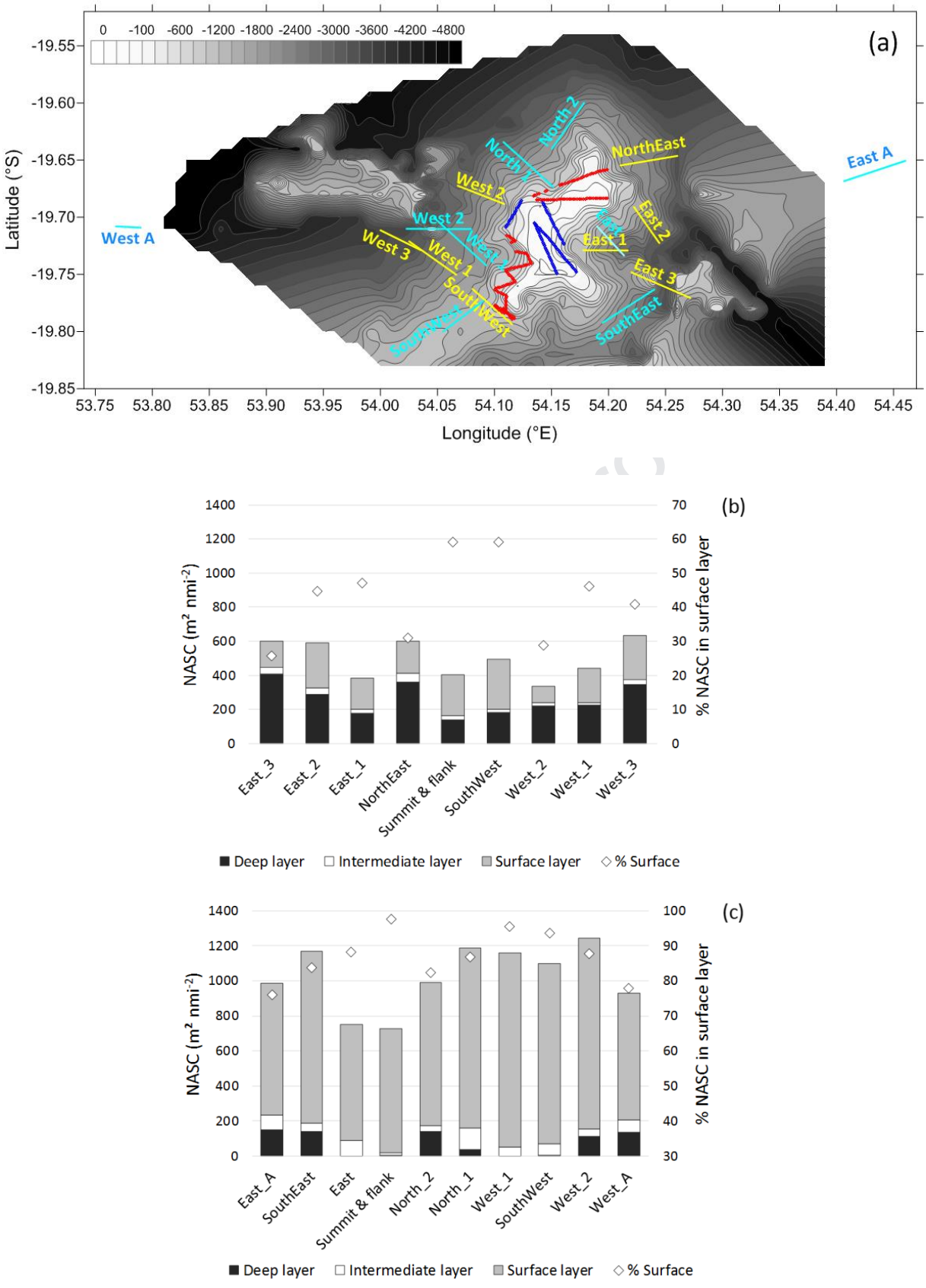
(a)
0 -100 -600 -1200 -1800 -2400 -3000 -3600 -4200 -4800
Latitude (°S)
Longitude (°E)
-19.55
-19.60
-19.65
-19.70
-19.75
-19.80
-19.85
53.75 53.80 53.85 53.90 53.95 54.00 54.05 54.10 54.15 54.20 54.25 54.30 54.35 54.40 54.45
West A
East A
North 2
North 1
NorthEast
West 2
West 2
West 3
West 1
West 1
South West
SouthWest
East 1
East 2
East 3
SouthEast
(b)
NASC (m² nmi⁻²)
% NASC in surface layer
East_3 East_2 East_1 NorthEast Summit & flank SouthWest West_2 West_1 West_3
Deep layer
Intermediate layer
Surface layer
% Surface
(c)
NASC (m² nmi⁻²)
% NASC in surface layer
East_A SouthEast East Summit & flank North_2 North_1 West_1 SouthWest West_2 West_A
Deep layer
Intermediate layer
Surface layer
% Surface

Figure 12

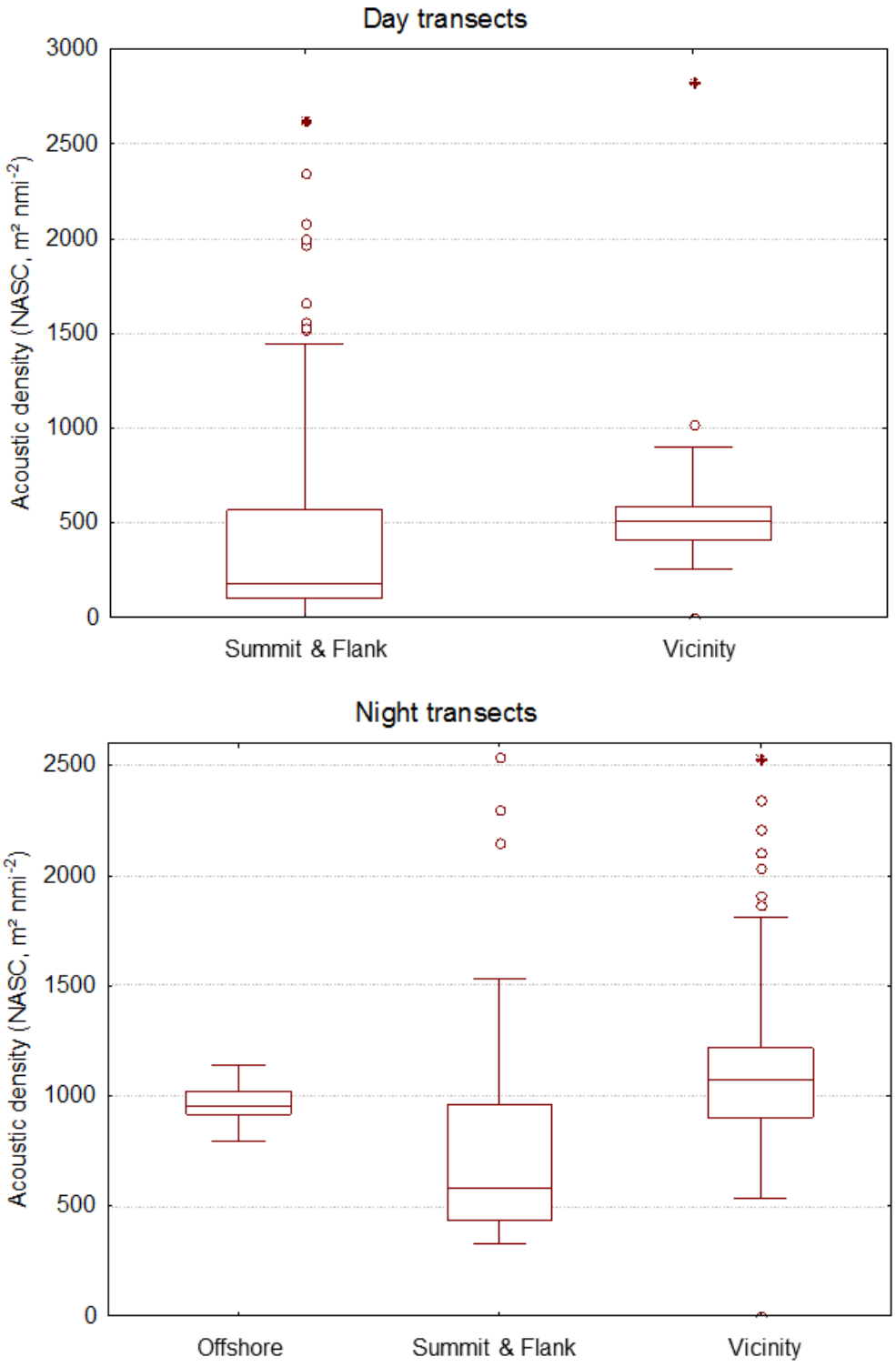
Day transects
Acoustic density (NASC, m² nmi⁻²)
3000
2500
2000
1500
1000
500
0
Summit & Flank
Vicinity
Night transects
Acoustic density (NASC, m² nmi⁻²)
2500
2000
1500
1000
500
0
Offshore
Summit & Flank
Vicinity

Figure 13

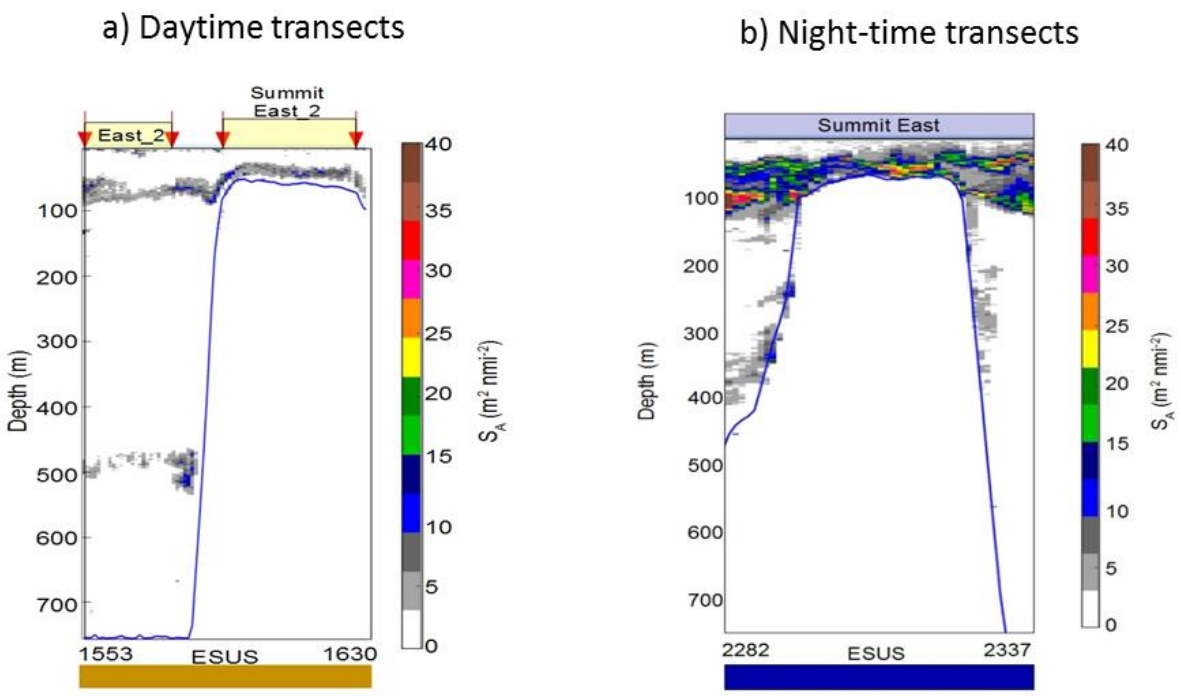

Figure 14

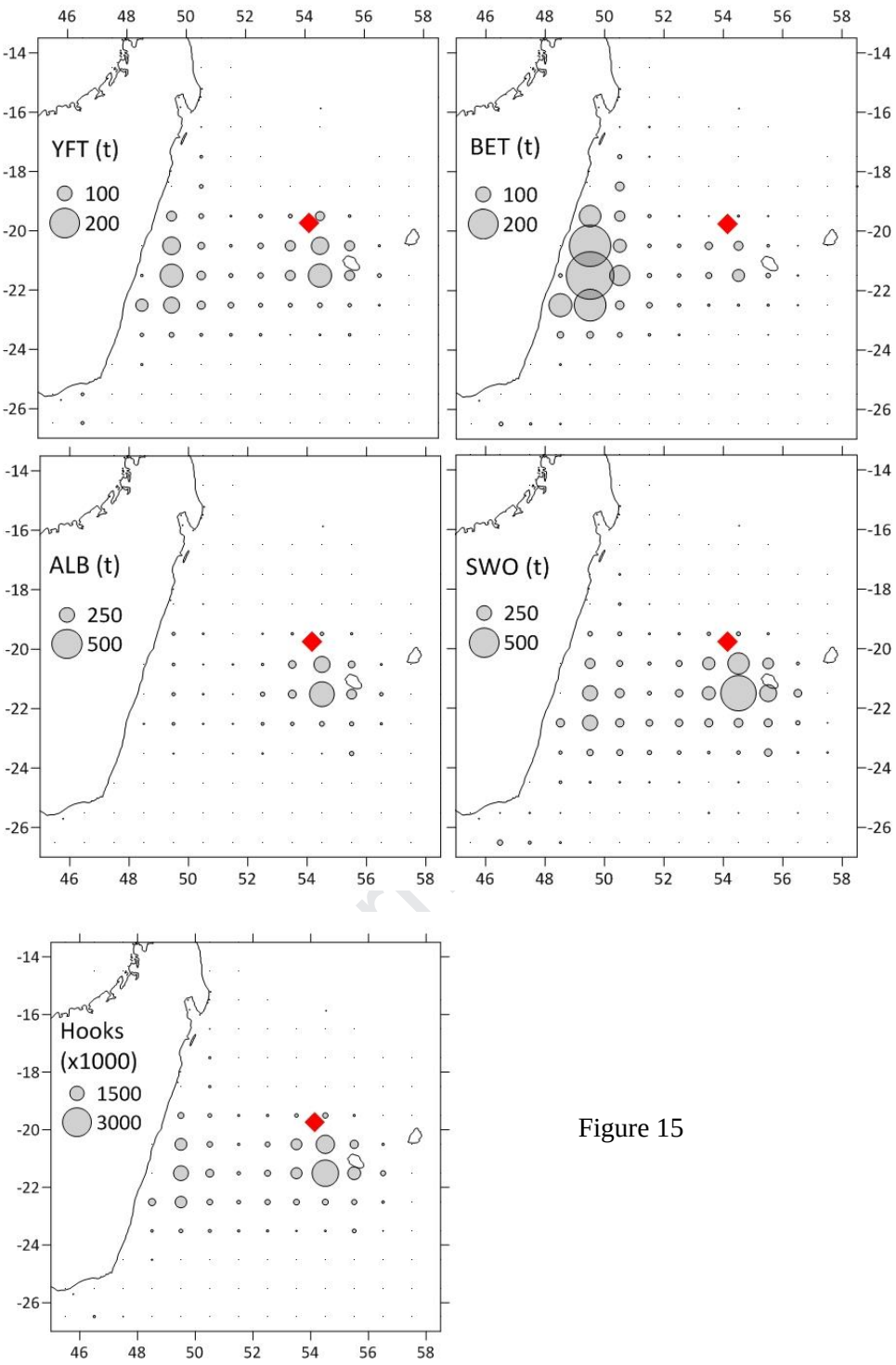
YFT (t)
100
200
BET (t)
100
200
ALB (t)
250
500
SWO (t)
250
500
Hooks
(x1000)
1500
3000
46
48
50
52
54
56
58
-14
-16
-18
-20
-22
-24
-26

Figure 15

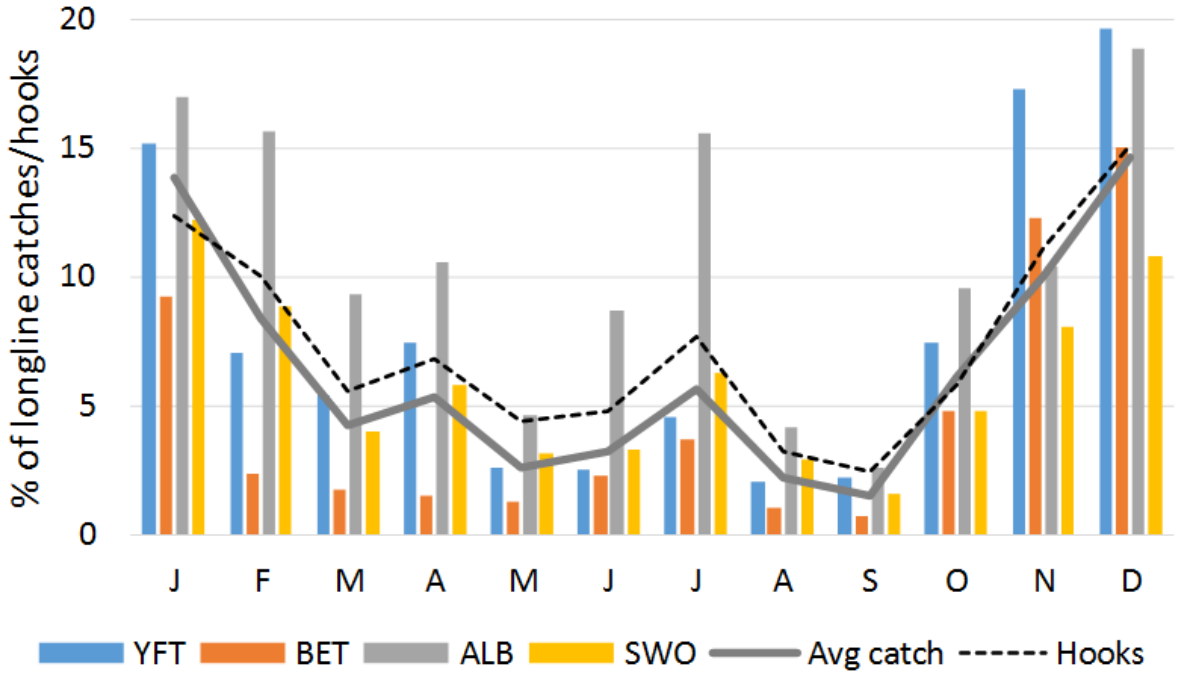

Figure 16

Declaration of interests – ms #137

☒ The authors declare that they have no known competing financial interests or personal relationships that could have appeared to influence the work reported in this paper.

☐The authors declare the following financial interests/personal relationships which may be considered as potential competing interests: